www.MaterialsViews.com

Boron Nitride Nanostructures: Fabrication, Functionalization and Applications

*Jun Yin, Jidong Li, Yang Hang, Jin Yu, Guoan Tai, Xuemei Li, Zhuhua Zhang, and Wanlin Guo**

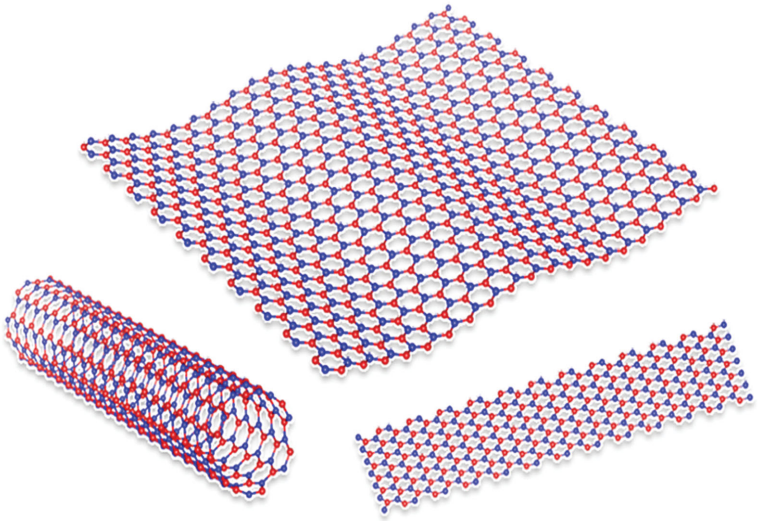

From the Contents

Boron nitride (BN) structures are featured by their excellent thermal and chemical stability and unique electronic and optical properties. However, the lack of controlled synthesis of quality samples and the electrically insulating property largely prevent realizing the full potential of BN nanostructures. A comprehensive overview of the current status of the synthesis of two-dimensional hexagonal BN sheets, three dimensional porous hexagonal BN materials and BN-involved heterostructures is provided, highlighting the advantages of different synthetic methods. In addition, structural characterization, functionalizations and prospective applications of hexagonal BN sheets are intensively discussed. One-dimensional BN nanoribbons and nanotubes are then discussed in terms of structure, fabrication and functionality. In particular, the existing routes in pursuit of tunable electronic and magnetic properties in various BN structures are surveyed, calling upon synergetic experimental and theoretical efforts to address the challenges for pioneering the applications of BN into functional devices. Finally, the progress in BN superstructures and novel B/N nanostructures is also briefly introduced.

1. Introduction

Boron nitride (BN) is a typical III-V group compound with a stoichiometry of boron and nitrogen being 1:1. Nitrogen occupies about 78% of Earth's atmosphere and is the most abundant uncombined element; whereas boron is a low-abundance element and mainly exists as borate minerals in nature. Although BN was not found in nature until 2009, when a cubic BN mineral was reported in Tibet of China, synthesis of BN has a long history and was first demonstrated by Balmain in 1842 through the reaction between boric acid and potassium cyanide.[1,2] During the past century, the fabrication of BN has been greatly developed, especially when hot pressing of BN was realized after 1960s. Nowadays, BN materials of different crystal structures have been widely used in many technological fields, such as lubricant by layered BN structures and abrasive by sphalerite BN crystal structure. Without BN additive, a lot of cosmetic products will lose their shining performance.

BN can be isomorphic to carbon in any lattice structure, from zero-dimensional (0D) cage, one-dimensional (1D) nanotube, two-dimensional (2D) monolayer to three-dimensional (3D) diamond-like crystal structure. Along with the advent of graphene, the 2D hexagonal BN (h-BN) has attracted particular research attention owing to a number of exceptional properties and immense potentials for diverse applications. Unlike purely covalent C–C bonds in graphene, the chemical bonds in h-BN monolayer show distinct ionicity, which localizes the electronic states and leads to superior chemical and thermal stabilities. Thus, h-BN nanosheets show unique potential for fabricating nanoscale devices operable in harsh environments and serving as high performance oxidation-resistant coatings. On the other hand, the bond ionicity breaks the symmetry of electronic states and opens a large band gap in the h-BN sheet, thus ending up with electrically insulating property. Current research into 2D h-BN still faces two great challenges: controlled fabrication of large-scale high-quality samples and effective electronic structure modulation towards tunable functionality.

Obtaining high quality h-BN samples requires the elimination of defects, especially grain boundaries stitching misoriented domains. To this end, h-BN single crystalline domains should either grow as large as possible or be well aligned with precisely the same orientations. The controlled growth of h-BN is contingent upon the full understanding of fundamental growth mechanism associated with different catalytic substrates. Moreover, extensive applications of h-BN need h-BN films with different thickness, which requires precise control of the layer number of h-BN sheets without compromising the crystallinity and uniformity. Besides, the past few years have also witnessed a rapid development in combining h-BN sheets with other 2D materials, such as graphene and 2D transition-metal dichalcogenide (TMDC), to form hybrid 2D materials. Controlled fabrication of the in-plane and vertical heterostructures with sharp and clean interface remains a task of great challenges. Considerable research attention has also been paid to 3D h-BN architectures comprised of 2D BN components, which promise the transfer of unique properties of h-BN nanosheets to macroscopic assemblies.

The h-BN sheet is the 2D building material for h-BN materials of all other dimensionalities. It can be tailored into 1D nanoribbons, wrapped into nanotubes, stacked into 3D h-BN crystals and assembled into various 3D structures. The synthesis methods, properties and potential applications of these BN nanostructures have been comprehensively reviewed.[3–5] It is concluded that the insulating property of h-BN sheet is robust against the changes in the dimensionality, which severely hinders the applications in functional devices. In the past decade, extensive theoretical research efforts have been devoted to modifying the electronic properties of various h-BN nanostructures. The electronic tunability of h-BN has been shown to rely not only on structural dimensionality, but also on chemical termination, bond configuration and the means of modulation. Theoretically, h-BN nanostructures can be tuned continuously from being insulating to semiconducting and even to metallic via various strategies. However, a gap between the theoretical prediction and experimental realization of electronic modulation prevents the realization of full potential of h-BN structures in functional applications. Innovative strategies for further optimizing their electronic modulations and improving the structural design of h-BN structures remain highly demanded.

In this review, we first review the progress of the synthesis, structural characterizations, tunable functionality and applications of 2D h-BN. Then we discuss the 1D nanoribbons and nanotubes, BN superstructures and novel B/N nanomaterials, focusing on the control of their functionalities. Finally we provide remarks on possible directions to move forward the BN research.

2. Synthesis, Properties and Applications of Two Dimensional h-BN

2.1. Synthesis

Various methods have been developed to fabricate 2D h-BN. Mechanical exfoliation provides h-BN flakes of the highest crystalline quality, which is particularly suitable for fundamental physical research.[16,17] The issue with this method is low yield and limited flake size less than tens of micrometers. Chemical exfoliation is an efficient way to fabricate few-layer h-BN flakes in large quantities.[18,19] However, this method suffers from surface contamination of the samples and even smaller flake size than that obtained through mechanical exfoliation. Besides, for both mechanical and chemical exfoliation,

Dr. J. Yin, J. Li, Y. Hang, J. Yu, Dr. G. Tai, X. Li,
Prof. Z. Zhang, Prof. W. Guo
State Key Laboratory of Mechanics
and Control of Mechanical Structures
Key Laboratory for Intelligent Nano Materials
and Devices of the Ministry of Education
Institute of Nanoscience
Nanjing University of Aeronautics and Astronautics
Nanjing 210016, P. R. China
E-mail: wlguo@nuaa.edu.cn

DOI: 10.1002/smll.201600053

the thickness of the h-BN flakes is of large variation. To resolve these problems, various methods have been applied to grow large area h-BN film of uniform thickness. Here, we mainly focus on the synthesis of large area h-BN films, its heterostructure and 3D architectures. A comprehensive summary of fabricating h-BN flakes by mechanical and chemical exfoliation can be found in previous reviews by Pakdel et al.[4]

2.1.1. Chemical Vapor Deposition

Chemical vapor deposition (CVD) on catalytic substrates has been widely adopted to grow large area h-BN films. The size of the obtained sample is only determined by the substrate size. The precursor can be gas (diborane and ammonia),[13] liquid (borazine)[6,12] and solid (ammonia borane).[9,7] To improve the quality and functionalities of the h-BN films, intensive research efforts have been paid to enlarge the grain size, fabricate h-BN film of desired layer numbers and precisely control the grain morphology and orientation. In this section, we review the progresses on these aspects in details.

2.1.1.1. Grain Size Control: The domain sizes of CVD grown h-BN were typically in the order of micrometer.[9] Reducing the precursor feeding rate proves to be an efficient route to increase the domain size of h-BN grown on Cu.[20–22] We recently showed that when the partial pressure of the gas precursor decomposed from ammonia borane was lowered from 3 Pa to 0.4 Pa, the average domain size increased from less than 1 μm to larger than 20 μm on the inside surface of a Cu tube (**Figure 1**a–c).[20] Similarly, Song et al. used a folded Cu enclosure approach to suppress the precursor feeding rate and improve the surface smooth.[21] The obtained single-crystalline domain size is up to 72 μm in edge length. Counterintuitively, Ning et al. reported that the domain size of h-BN increases with the provided content of ammonia borane.[22] This may be attributed to their specifically designed CVD chamber. The h-BN domain size can also be enlarged by improving the surface flatness, which was realized by electropolishing and long pre-annealing treatment of the Cu substrate.[23,24]

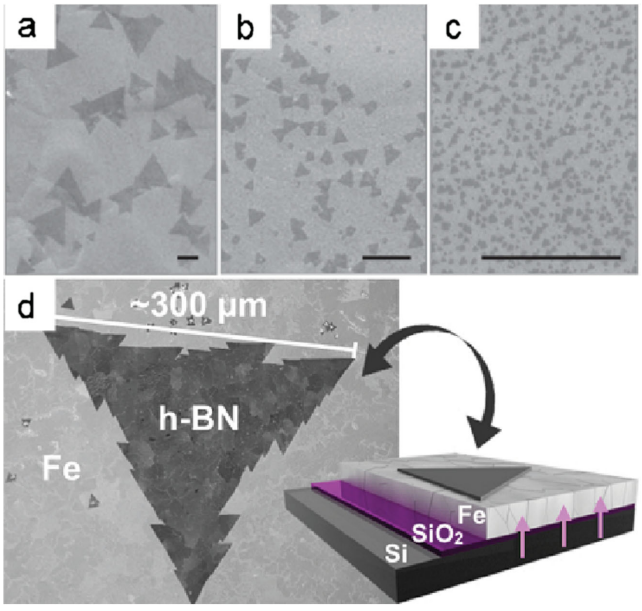

Figure 1. Grain size control of CVD h-BN. a–c) Scanning electron microscopy (SEM) images of h-BN grains grown under different precursor partial pressure, 0.4, 1, and 3 Pa for (a, b and c), respectively. Scale bars, 10 μm. Reproduced with permission.[20] Copyright 2015, Wiley-VCH. d) SEM image of a large, tooth-edged h-BN domain grown on $Fe/SiO_2/Si$ substrates, which is schematically illustrated in the insert. Reproduced with permission.[25] Copyright 2015, American Chemical Society.

Although the grain size of h-BN has been significantly enlarged through delicate control of relevant parameters, it is still much smaller than that of graphene grown on Cu foils, whose diameter can exceed 1 cm.[26] This may be attributed to the high chemical affinity of N-containing intermediate species to the Cu surface.[21] Thus, special design of the substrate is required for further enlarging the h-BN domain size. Lu et al. demonstrated that the nucleation density can be greatly reduced to 60 per mm^2 by introducing Ni into the Cu substrates, and the single-crystal h-BN grains can grow to 7500 μm^2 under the optimized condition.[27] They attributed this to the Ni assisted decomposition of poly aminoborane nanoparticles on the substrate surface during the growth. Caneva et al. took a simple thin-film $Fe/SiO_2/Si$ catalyst system and successfully grew monolayer h-BN single crystals with lateral dimensions of ≈0.3 mm (Figure 1d).[25] In this method, controlled Si diffusion into the Fe catalyst allows exclusive nucleation of monolayer h-BN with very low nucleation densities. The underlying mechanism is proposed as that the incorporated Si reduces the supersaturation required to nucleate h-BN, thus the onset of nucleation is reduced and the precursor supply feeds fewer nuclei.

2.1.1.2. Grain Morphology Control: For CVD-grown sample, h-BN domains usually adopt triangle shape, instead of the hexagonal shape observed for graphene.[28] Besides h-BN triangles, Kim et al. observed an asymmetric diamond shape under high baking temperature of the ammonia borane precursor.[9] The origin of this shape remains unclear. Tay et al. compared the h-BN domains grown on unpolished and electropolished Cu foils under atmospheric pressure, and found that the h-BN domains grown on electropolished Cu foils adopted a hexagonal shape.[23] They attributed this to the abundance of surface oxygen on the polished Cu surface. It

Wanlin Guo received his PhD from Northwestern Polytechnic University in 1991, and then worked as postdoctoral researcher, associated professor and professor in Xi'an Jiaotong University. In 2000, he joined Nanjing University of Aeronautics and Astronautics as Chair Professor Position of the Education Ministry of China. He is now the director of the Key Laboratory for Intelligent Nano Materials and Devices of the Ministry of Education, and Institute of Nanoscience in Nanjing University of Aeronautics and Astronautics. His research is focused on nanoscale physical mechanics, intelligent nanomaterials and devices, high efficient energy conversion nanotechnology, three dimensional fatigue fracture, damage tolerance and durability design of structures.

is also found that, by increasing the Ar annealing time prior to h-BN growth, the h-BN shape varied gradually from triangular, trapezoidal, hexagonal to complex shapes.[29] Residual oxygen in the CVD system was proposed to oxidize the Cu surface and account for the observed shape variation. Using a wedge-shaped Cu pocket with two opened ends, we demonstrated that h-BN triangles grown on the inside of the pocket gradually evolve to truncated-triangles and then to hexagons with decreasing the gap distance between the top and bottom Cu foil (**Figure 2**a–e).[20] Since the h-BN triangles and hexagons appear on the same piece of Cu foil, surface oxygen is eliminated as the possible reason. We proposed that the enhanced copper vapor pressure may play an important role here. The shape-evolution from triangle to truncated-triangle and further to hexagon was also observed with the increase of distance from Cu substrate to the precursor, and was attributed to the deficiency of nitrogen activate species farther to the precursor.[30] This kind of substrate position effect was also observed on resolidified copper surface.[31] In situ observation of h-BN growing on Ru (0001) revealed that the morphology of h-BN is also ultrasensitive to H_2.[32] Without introducing H_2, the growth speed of h-BN along the steps on the substrate surface is substantially faster than that across steps, resulting anisotropic wire-like h-BN domains. With concurrent exposure to borazine and H_2, the individual domains grow more slowly, and they assume compact shapes with nearly isotropic growth rate, regardless of the underlying Ru steps. The potential origins include hydrogen-induced modification of the states of Ru step edges and the diffusion of surface species.

Several theorical works have been conducted to explain the morphology of h-BN.[33,34] Based on crystal growth theory augmented by detailed first-principles calculations, Zhang and co-workers revealed an atomistic growth mechanism of h-BN based on nonequilibrium dynamics near the growing edge. The result shows a strong kinetic anisotropy of growth at the h-BN edges and yields an island shape varying from regular triangle, truncated triangle to hexagon relying on the chemical potential (μ) of feeding species (Figure 2f–i), explaining a number of experimental phenomena discussed before. In contrast to previous common vision, the predicted thermodynamically optimal shapes of h-BN island mostly differ from those in experimental observations.

2.1.1.3. Grain Orientation Control: Electrical performances of graphene supported on h-BN show notable dependence on their relative lattice orientation.[35,36] To realize the fabrication of devices with uniform desired performance,

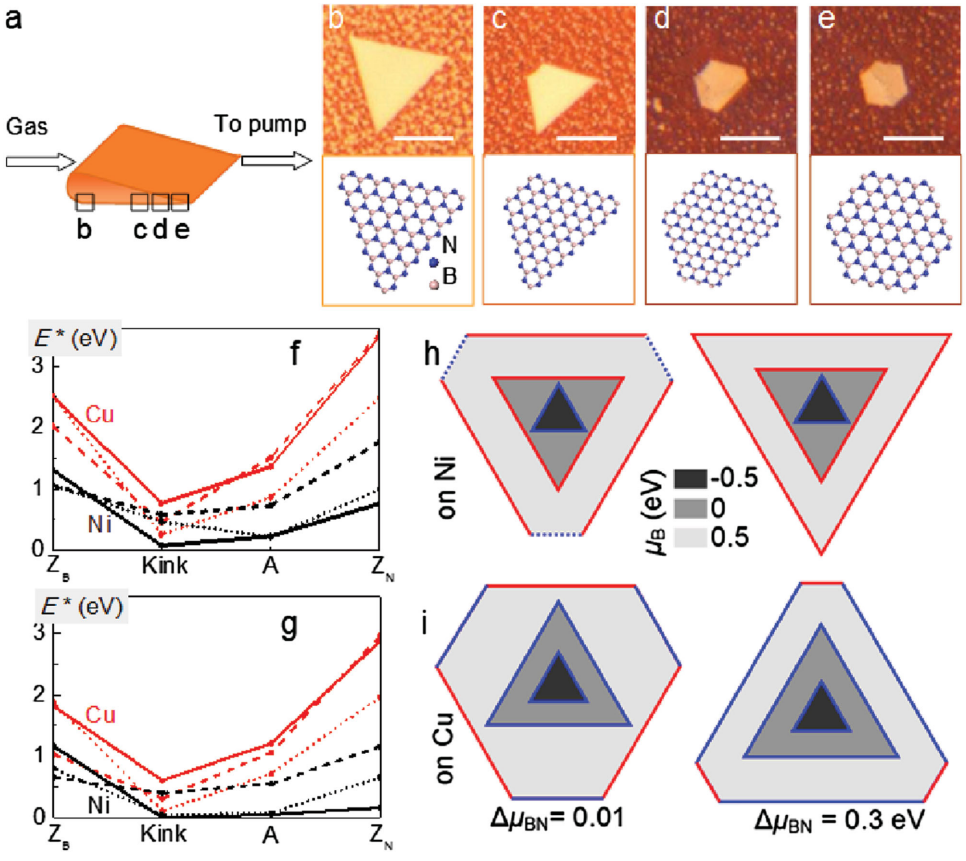

Figure 2. Grain morphology control of CVD-grown h-BN. a) Configuration of the Cu pocket for the growth of h-BN. b–e) Optical images of typical h-BN grains at different locations marked in (a). Reproduced with permission.[20] Copyright 2015, Wiley-VCH. f–i) Kinetic growth of h-BN domain. Free energy barriers for nucleating atomic rows at principal h-BN edges at $\mu_B = -0.5$ (dashed lines), 0 (solid lines) and 0.5 eV (dotted lines) on Cu (wine lines) and Ni (black lines), at $\Delta\mu_{BN} = 0.01$ eV (f) and 0.3 eV (g). Shapes from kinetic Wulff construction for h-BN on Ni (h) and on Cu (i) at selected μ_B and $k_BT = 0.1$ eV. The results at $\Delta\mu_{BN} = 0.01$ and 0.3 eV are shown in left and right panels, respectively. The red, blue and black lines represent the standard Z_B, Z_N and A. Reproduced with permission. [33] Copyright 2016, American Chemical Society.

preparation of h-BN with controlled orientation is required. The epitaxy of h-BN on single-crystal substrates has been extensively explored. It is shown that the lattice orientations of h-BN are generally predefined with respect to the substrate lattice despite their weak van der Waals (vdW) interaction.

Works on epitaxial growth of h-BN are mainly focused on (111) facets of various transition metals with face-centered cubic structure. Four sets of stacking structure, named here as R-0, R-30, R-60 and R-90, respectively, are commonly observed (**Figure 3**a). On Ni (111), h-BN monolayers with primary R-60 structure were synthesized using borazine as precursor,[37–39] consistent with the density functional theory (DFT) calculations. However, the energy difference between R-0 and R-60 is very small and can be easily overcome at the growth temperature, making the R-0 an alternative orientation sometimes.[40–42] Moreover, Auwärter et al. revealed that the ratio of R-0 and R-60 structures on Ni (111) could be modulated by pretreating the Ni substrates, but the deep mechanism is unclear.[42] Besides, through changing the precursor dosing manner, h-BN of unique orientation can be grown on Ir (111) substrate.[43] Only R-60 h-BN domains grow on Ir (111) by dosing borazine at low temperature and subsequent high temperature annealing, but R-60 and R-0 domains coexist if borazine is dosed directly at high-temperature.[43] The R-60 structure is also commonly found on Rh (111) and Ru (0001), where h-BN monolayers are bonded on these surfaces much more strongly.[44] However, for weakly interacted substrate, such as Cu (111), Au (111), Pt (111) and Pd (111), both the R-0 and R-60 are dominant structures.[21,45,46] In particular, additional R-30 and R-90 domains could appear for h-BN grown on Pt (111) and Pd (111).[47,48] When the interaction between h-BN and metal becomes even weaker, as in the case of Ag (111), no preferred orientation can be found.[49]

For large scale application, noble metal substrates are not preferred. It has been reported that, through long term annealing or resolidification, Cu (111) and Cu (110) single crystal can be easily prepared to grow aligned h-BN with two primary orientations.[31,51] We also have shown recently that highly aligned h-BN can be epitaxially grown on semiconducting Ge substrates of (100) and (110) facets. It is shown that the number of primary orientations of the h-BN domains is notably dependent on the symmetry of the underlying crystal face. Two and four primary orientations are observed on Ge (110) and Ge (100), respectively (Figure 3b–e).[50] It has been proven that h-BN flakes of the same orientation can merge seamlessly without structural domain boundaries, convincing that it is a potential way to fabricate single crystalline h-BN film.[29,50] However, to reach this goal, further efforts are called upon to eliminate the oppositely orientated domains and realize the growth of uniformly orientated h-BN.[50]

2.1.1.4. Layer Number Control: When serving as a tunneling barrier, the thickness of the ultrathin h-BN film needs to be precisely controlled with atomic uniformity. To efficiently block the scattering effects from the underlying impurities, h-BN substrate with thickness more than ten nanometers is desired. Thus, controlling the layer number of h-BN film is very important for its practical applications in electrical devices. Similar to the growth of graphene on Cu,[52] the decomposition of precursor mainly occurs on the catalytic metal surface, and the h-BN grown on Pt surface at low pressure are self-limited to monolayer without the associating precipitation (**Figure 4**a).[6,7] However, under ambient pressure, the layer number of h-BN grown on Pt increases from monolayer to few layer with the increase of precursor concentration (Figure 4b), and is not self-limited.[8] At relative low precursor concentration, monolayer h-BN growth

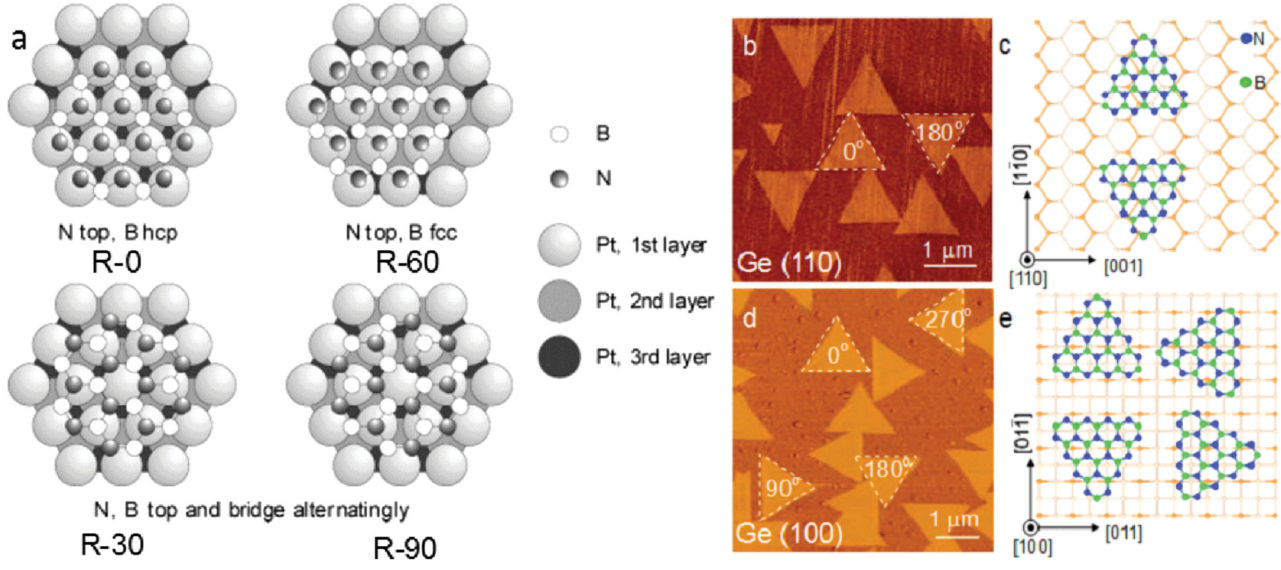

Figure 3. Epitaxial growth of h-BN with preferred orientations. a) Four typical stacking structures of h-BN epitaxially grown on Pt (111). Reproduced with permission.[47] Copyright 2005, American Chemical Society. b,d) Friction force images of h-BN triangles grown on Ge (110) (b) and (100) (d), respectively. c,e) Schematic illustration of the deduced orientations of the h-BN domains with respect to the underlying Ge (110) (c) and (100) (e) substrates. Reproduced with permission.[50] Copyright 2015, Wiley-VCH.

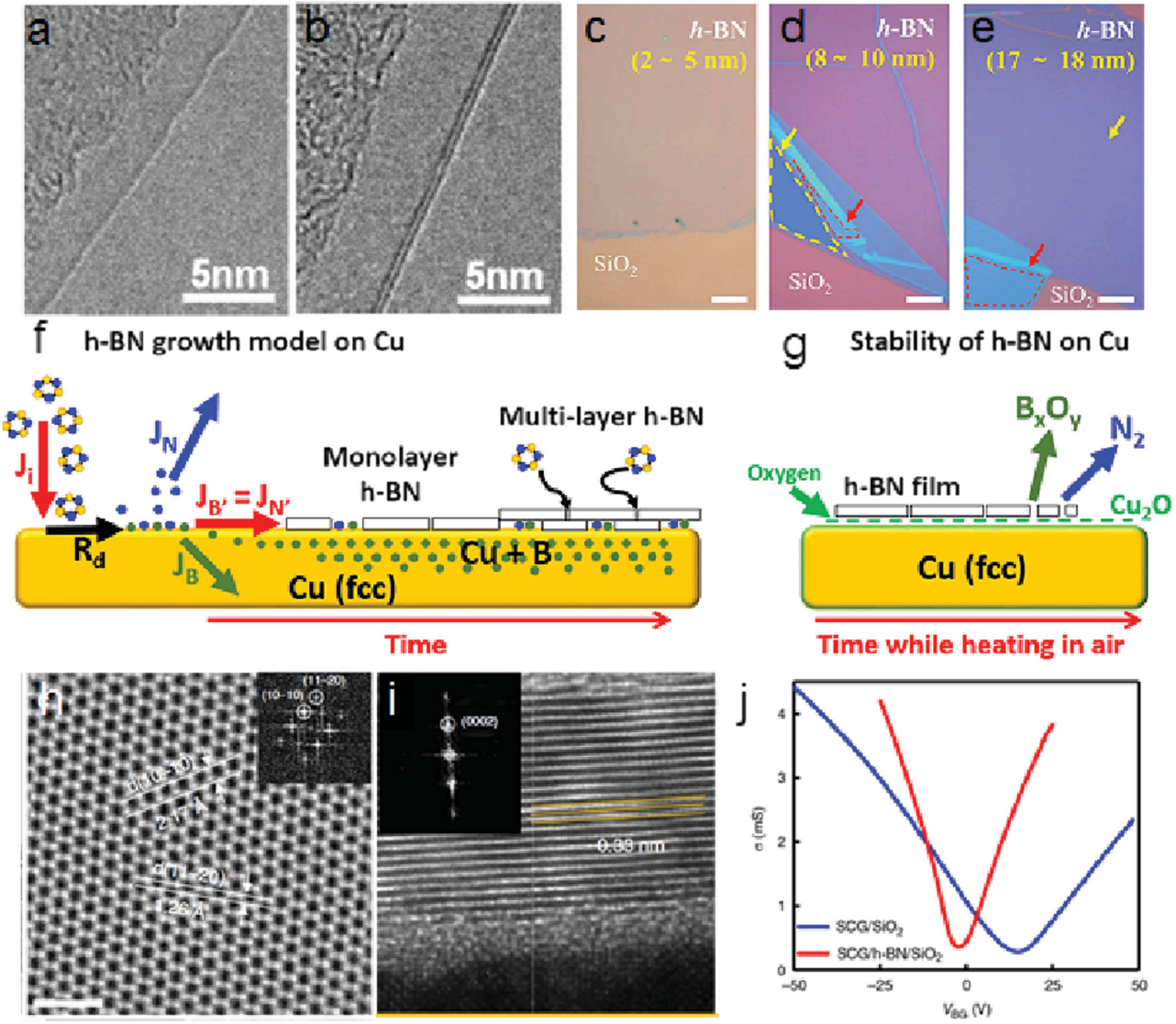

Figure 4. Layer number control of CVD-grown h-BN. a,b) Transmission electron microscope (TEM) images of monolayer and bilayer h-BN films grown on Pt substrate. Reproduced with permission.[8] Copyright 2013, American Chemical Society. c–e) Optical images of h-BN films with different thicknesses on a SiO_2/Si substrate. Reproduced with permission.[12] Copyright 2012, American Chemical Society. f) Schematic diagram for h-BN growth mechanism on Cu. g) Schematic diagram for stability of h-BN on Cu and the oxygen-mediated catalytic dissociation mechanism. Reproduced with permission.[54] Copyright 2014, American Chemical Society. h,i) TEM image of an as-grown multilayer h-BN film (h) and its cross-sectional (i) image on a Fe foil. j) The representative conductance (σ) of the graphene channel as a function of applied back gate (V_{BG}) on SiO_2 and on h-BN/SiO_2 substrates. Reproduced with permission.[15] Copyright 2015, Nature Publishing Group.

follows a Frank van der Merwe model due to the adatom-surface interaction. At relative high precursor concentration, few layer nuclei form, followed by lateral growth and formation of few layer films. In addition, with the extension of the growth time, additional layers grow on the continuous h-BN film following a Stranski-Krastanov model. It is similar for the growth of monolayer h-BN on Cu under low pressure CVD.[9] Not only on Pt, the layer number of h-BN grown on Cu also seems to be sensitive to the chamber pressure.[9,10] Similarly, low pressure CVD growth mainly gives rise to monolayer h-BN,[9] ambient pressure CVD growth results in few layers (**Table 1**).[10,53,11] Kim et al. even showed that, using borazine as precursor, h-BN film with thickness between 2 to 20 nm and grain size around 10 nm can be deposited on Cu at 750 °C under ambient temperature (Figure 4c–e).[12] The reason of pressure dependence of h-BN layer number is not very clear at this stage, and needs to be explored with a deep understanding of the growth mechanism. The diffusion length and concentration of the precursor on the metal surface should play an important role.

To explore the growth mechanism of h-BN on Cu, Kidambi et al. utilized in situ X-ray photoelectron spectroscopy and X-ray diffraction to reveal the surface states at different growth stages.[54] They found that the nucleation and growth of h-BN layers was isothermal. However, in contrast to the surface-mediated graphene CVD growth, B is found to be incorporated into the Cu bulk during borazine exposure (Figure 4f), introducing a Cu lattice expansion and B precipitation from Cu upon cooling, while N incorporation is not observed. They suggested that additional layers nucleated

Table 1. Summary of factors in relation with the layer number of obtained h-BN.

Substrate	Pressure (mTorr)	Thickness	Precursors	Determinant
Pt[6]	<100	monolayer	borazine	–
Pt[7]	100	monolayer	ammonia borane	–
Pt[8]	Ambient pressure	mono to few layers	ammonia borane	precursor concentration
Cu[9]	350	monolayer	ammonia borane	–
Cu[10]	Ambient pressure	2–5 layers	ammonia borane	–
Cu[11]	Ambient pressure	6–8 layers	ammonia borane	–
Cu[12]	Ambient pressure	2–20 nm	borazine	growth time
Ni[13]	135	1–100 layers	diborane and ammonia	growth time
Ni[14]	Ambient pressure	5–50 nm	borazine	precursor concentration and growth time
Fe[15]	low pressure	5–15 nm	borazine	Cooling rate

and grow only at the interface between the catalyst and the first h-BN layer, with feeding through the inherent defects in the h-BN layer (Figure 4f). Furthermore, they also demonstrated that oxygen molecular could facilely intercalate into the interface between as-grown h-BN and Cu substrate during ambient air exposure (Figure 4g).

The growth behavior of h-BN shows significant difference on different metal substrate. Using diborane and ammonia as the gas precursors, layer number of h-BN grown on Ni foil by low pressure CVD is linearly dependent on the growth time.[13] Few-layer h-BN was also grown by a sequential growth method, similar to atomic layer deposition.[13] Although a complete understanding of the growth mechanism is lacked, nucleation by the reaction of Ni and B was suggested to be crucial here. Shi et al. demonstrated that, through low-temperature deposition of precursors followed by a post annealing process,[14] large-area h-BN film with a thickness between 5 and 50 nm could be deposited on Ni surface at ambient pressure. Recently, Fe foil was used as an promising substrate to grow multilayer h-BN in a segregation mode through CVD (Figure 4h, i).[15] Boron and nitrogen atoms being precipitated in Fe substrate at high temperature will segregate to form h-BN film during the cooling process. The thickness of h-BN film is in the range of 5–15 nm, which is controlled by the cooling rate. The grain size of h-BN film was estimated to be at least 40 000 μm^2, and the reported graphene mobility of 24 000 $cm^2 V^{-1} s^{-1}$ at room temperature is the highest value among previous reports with CVD-grown graphene samples on CVD-grown h-BN substrates (Figure 4j).

2.1.2. Other Methods for Fabrication of Large Area h-BN Films

A practical problem during the CVD growth of h-BN is the use of some unconventional precursors as mentioned above. These compounds are rare and highly toxic, unstable, or pyrophoric. To resolve this problem, Wang et al. utilized ion beam supporting deposition to grow h-BN on Cu foil.[55] The precursor is provided by directly sputtering a h-BN target with an Ar ion beam. The h-BN domain morphology fabricated by this method shows notable dependence on the deposition atmosphere and growth temperature. The nucleation density can be significantly decreased by a in situ pre-etching of Ni substrate and reducing the concentrations of active species, enabling the growth of h-BN domain with edge length up to 100 μm.[56]

Currently, high-quality h-BN bulk crystals is typically produced by a recrystallization process using metal solvent at high temperature.[57–59] Inspired by this process, Zhang et al. developed a co-segregation method to synthesize wafer-scale h-BN thin films with thickness ranging from sub-monolayer, monolayer to multilayer (**Figure 5**a,b).[60] They designed a sandwiched substrate with a solid-state (B,N)-layer between an Fe top layer and a Ni bottom layer. Following the dissolution of B and N into the metal at high temperature, h-BN film automatically segregates on the metal surface during the cooling process. This method follows an underneath-growth model, and enables the predefining the thickness and location of the h-BN film by pre-patterning the solid (B,N)-source.

Physical vapor deposition is another scalable method to produce few-layer BN films with good thickness uniformity.[61] Sutter et al. demonstrated the growth of few-layer h-BN films with controlled thickness on Ru (0001) surface by magnetron sputtering of B in N_2/Ar (Figure 5c,d). h-BN films up to two atomic layers can be synthesized by reactive deposition at high temperatures. Thicker h-BN films can be obtained by cycles of alternating room temperature deposition and annealing. Furthermore, the insulating property of the h-BN film was evaluated by tunneling transport across the films, demonstrating a pinhole-free insulating behavior.

2.1.3. Synthesis of 2D Heterostructures Involving h-BN

Stimulated by the attractive performances of vertical and in-plane heterostructures of 2D materials involving h-BN, intense attentions have been paid to construct these heterostructures with a precise control of the structure and interface. Graphene/h-BN vertical heterostructures were first realized by manually stacking of exfoliated graphene and h-BN flakes through a polymer mediated process.[62] Although this method has been further developed and is viable regardless of the specific stacking materials and sequences, it is time consuming and not practical for large scale applications.[63,64] Stacking CVD samples together through sequential transfer is a facile way to realize large area fabrication. However, organic and metallic contaminants are unavoidable during the transfer process,[65,66] which would significantly depress the intrinsic performances. To resolve this problem, 2D heterostructures need to be directly synthesized on the same substrate sequentially. It has been proved that graphene can be epitaxially grown on exfoliated h-BN flakes with exceptional high quality by CVD (**Figure 6**a–c), with mobility around 30 000 $cm^2 V^{-1} s^{-1}$.[67–69] Introducing silane as gaseous catalyst, the growth rate can be improved from 1 nm min^{-1} to 1 μm min^{-1}.[70] Furthermore, it was demonstrated that

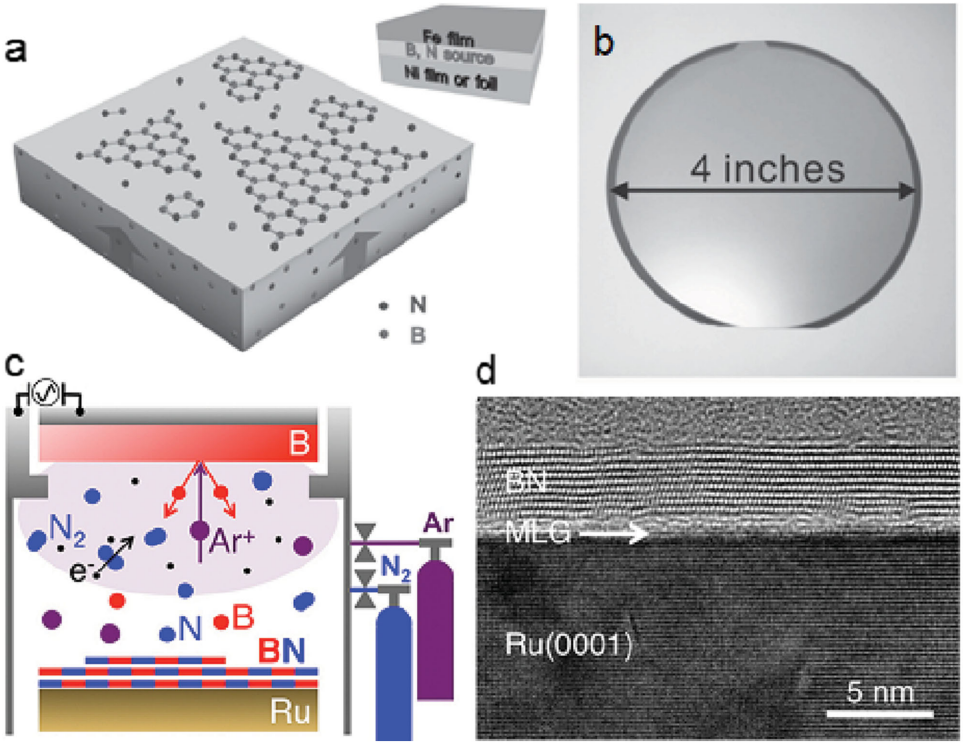

Figure 5. Co-segregation and physical vapor deposition of h-BN film. a) Schematic of h-BN synthesis by the vacuum annealing of sandwiched substrates Fe/(B,N)/Ni. b) Photograph of a h-BN film grown on a 4-inch substrate. Reproduced with permission.[60] Copyright 2014, Wiley-VCH. c) Schematic diagram of the planar magnetron geometry for deposition from a solid boron target in Ar/N_2 gas. d) TEM image of a 10-layer BN film deposited on Ru (0001). Reproduced with permission.[61] Copyright 2013, American Chemical Society.

graphene can be deposited on CVD-grown h-BN,[71–73] or vise verse, realizing the large area fabrication.[74,75] It is demonstrated that monolayer h-BN on Cu shows higher catalytic activity than bilayer h-BN for graphene.[76] Zhang et al. also developed a co-segregation method to directly synthesize wafer-scale graphene/h-BN films.[77] They annealed a sandwiched growth substrates (Ni(C)/(B,N)-source/Ni) in vacuum, and then gradually cooled the chamber, letting the

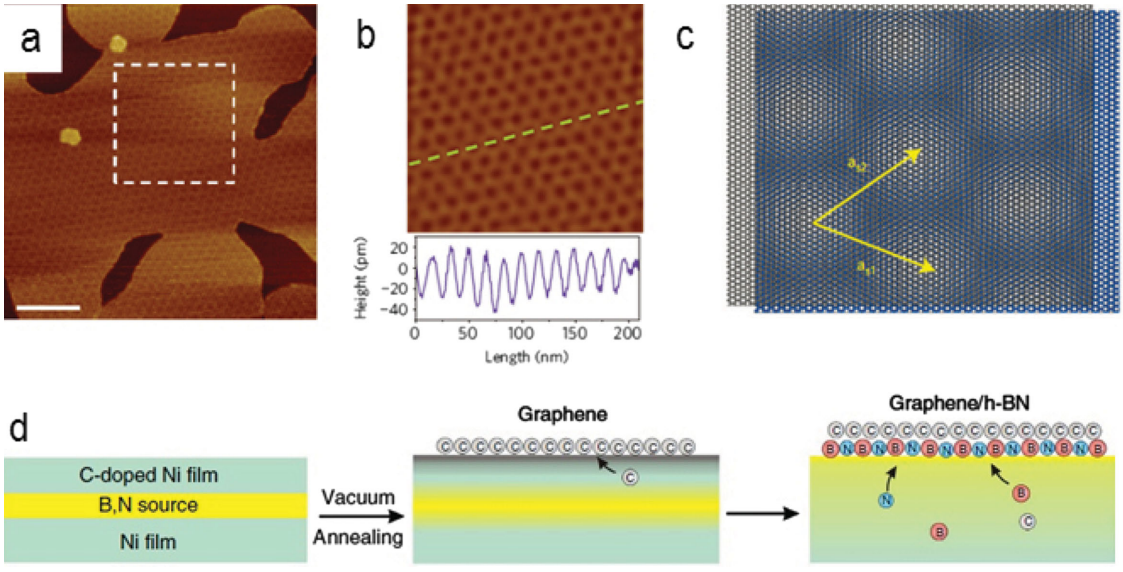

Figure 6. Synthesis of vertical graphene/h-BN heterostructure. a) Moiré pattern of a coalesced graphene grain on h-BN. b) High-pass-filtered inverse fast Fourier transform of the pattern in the dashed square in (a) and the lower part is the height profile along the dashed line. c) A schematic illustration of the moiré pattern generated by lattice mismatch with zero rotation angle. Reproduced with permission.[67] Copyright 2013, Nature Publishing Group. d) Schematic illustration of the co-segregation growth process for graphene/h-BN heterostructures. Reproduced with permission.[77] Copyright 2013, Nature Publishing Group.

segregation of graphene and h-BN, sequentially (Figure 6d). However, regardless of which method is adopted, the quality of the obtained graphene on synthesized h-BN films is far away from that grown on exfoliated h-BN flakes, with mobility ranging from 1.5 $cm^2 V^{-1} s^{-1}$ to 3000 $cm^2 V^{-1} s^{-1}$,[72,77] mainly due to the limited quality of deposited h-BN, cross doping and impurity at interface. Not only graphene, other kinds of 2D materials, such as MoS_2, can also be deposited on h-BN.[78] Actually, it is much easier to grow TMDCs on h-BN compared to graphene as no catalysts is required for the growth of TMDCs, whereas the quality of deposited TMDCs on h-BN needs to be elucidated.

Distinguished from the vertical heterostructures, which is hold together by vdW force, in-plane heterostructures are connected by covalent bonds, thus asking for a similar structure and lattice constant between the two constitutive materials. Only graphene is demonstrated to be able to form in-plane heterostructures with h-BN till now. Generally, there are three strategies to fabricate inplane h-BN/graphene heterostructures by CVD. First, h-BNC material, consisting of hybridized domains of h-BN and graphene can be directly deposited on Cu foils by simultaneously introducing methane and ammonia borane.[79] The graphene and h-BN domains are randomly distributed and of size only several nanometers. Second, h-BN/graphene heterostructures with larger h-BN and graphene domains can be synthesized by partially exposed growth, wherein partially exposed substrates are obtained by patterned etching of the continuous graphene/h-BN film (**Figure 7**a–c),[80,81] or partial growth (Figure 7d–i).[76,82–86] Alternatively changing the introduced source, graphene ribbon arrays with width below 100 nm can be obtained. Since the inter-edge between graphene and h-BN tends to be zigzag edge (Figure 7d–i),[83] it is possible to fabricate zigzag graphene nanoribbon without dangling edges and impurity scatterings through this methods. Third, graphene can be selectively converted to h-BN layers by substitution reaction and vice versa.[87,88]

The growth of vertical and in-plane heterostructures of graphene and h-BN can be switched just by controlling the growth temperature.[89] It is realized by turning on/off the h-BN etching reaction with CO_2 molecules, which is decomposed from benzoic acid during the growth of graphene. At a temperature over 900 °C, the etching reaction is turned on, giving rise to the in-plane graphene growth. In contrast, at a relatively low temperature, the etching reaction is turned off, leading to the vertically epitaxial growth of graphene.

2.1.4. Construction of 3D Materials from h-BN Flakes

Three-dimensional architectures consisted of h-BN flakes are versatile for practical applications in electronics, catalysis devices, sensors and adsorption materials. A lot of efforts have been paid to fabricate 3D h-BN architectures, and the obtained materials show a variety of outstanding properties.

In 2013, we fabricated 3D hierarchical h-BN foam through low pressure CVD using nickel foam as the template.[90] The 3D h-BN foam shows a hierarchical structure (**Figure 8**a) and promising outstanding properties, including low density down to 1.6 mg cm^{-3}, permittivity of 1.03 times that of air, and thermal stability up to 1200 °C. It can completely recover its original shape after cyclic compression exceeding 70% (Figure 8b,c) with permittivity within 1.12 times that of air (Figure 8d), complementing the conductive properties of carbon and metal based ultralight materials.[91,92] The thickness of the branch wall synthesized by this method is several nanometers, which can be significantly increased to hundreds of nanometers through ambient pressure CVD.[93] Following our work, Loeblein et al. fabricated 3D BN–C architecture

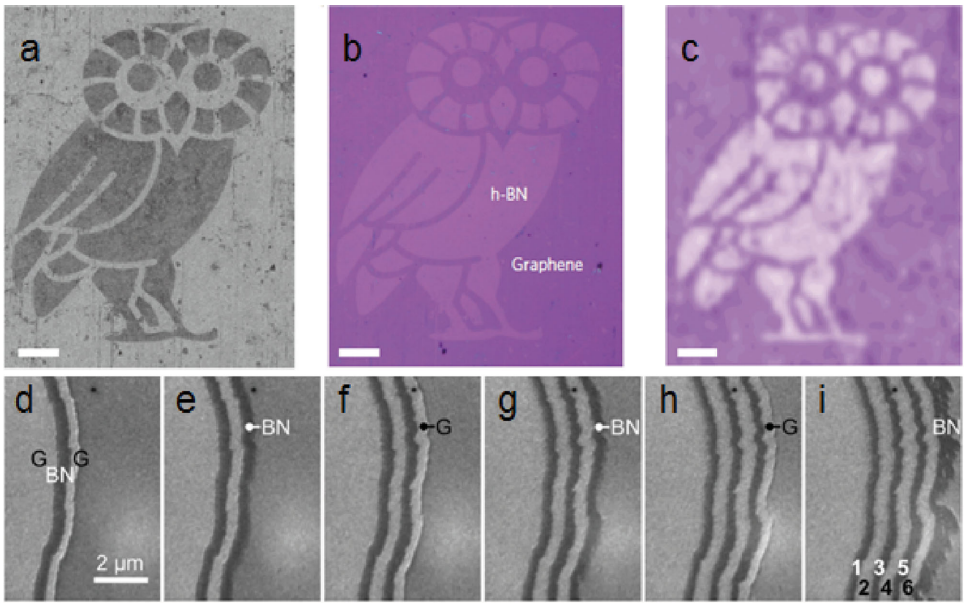

Figure 7. Synthesis of in-plane graphene/h-BN heterostructure. a–c) SEM image, optical image and Raman mapping of micrometer-sized owl pattern of graphene/h-BN in-plane heterostructure. Reproduced with permission.[81] Copyright 2013, Nature Publishing Group. d–i) Real-time microscopy of the stepwise growth of a monolayer superlattice of alternating graphene (G) and h-BN stripes on a Ru (0001) substrate. Reproduced with permission.[86] Copyright 2014, American Chemical Society.

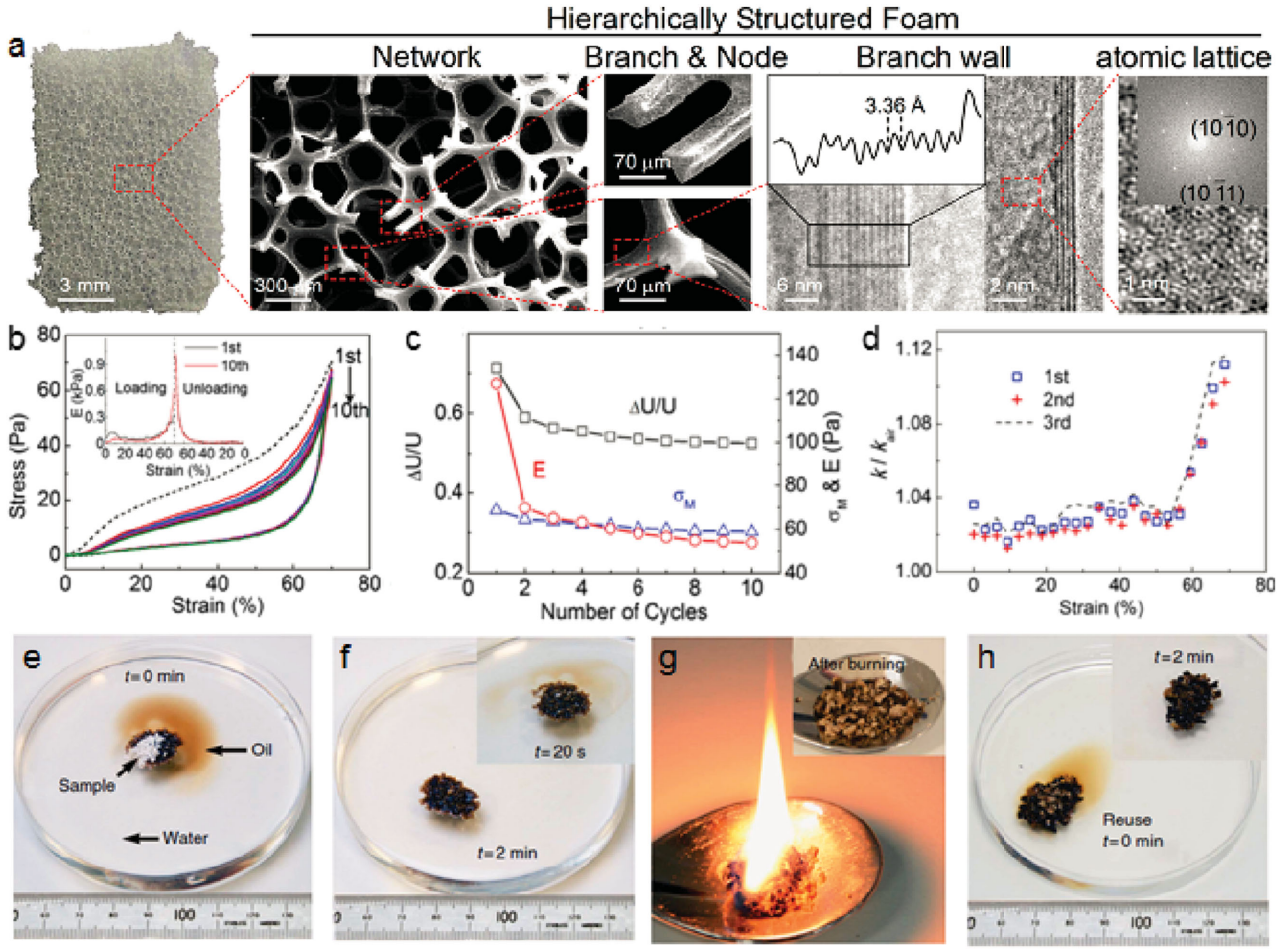

Figure 8. Structure, properties and applications of 3D h-BN. a) Hierarchical structures of the free-standing h-BN foam. b) Fatigue resistance of h-BN foam to cyclic compression to 70% strain. c) History of the maximum stress (σM), compressive modulus (E), and energy loss ratio during the 10 cycles shown in (b). d) Permittivity of the BN foam relative to air as a function of strain in three compressing cycles to 70% strain. Reproduced with permission.[90] Copyright 2013, American Chemical Society. e–h) Series images of oils absorption, removing and reuse of porous h-BN. Reproduced with permission.[98] Copyright 2013, Nature Publishing Group.

via a two-step growth of h-BN and graphene on nickel template, separately.[94] Through adjusting the C:BN composition, the 3D-BNC composite shows high tunability in electrical conductivity and electromagnetic interference shielding effectiveness. The composite maintains a very high thermal diffusivity, being an ideal candidate for electronics packaging. Not only on metal template, h-BN can also be deposited on graphene-carbon nanotube composite aerogels and carbonaceous template starting from zeolite.[95,96] To get freestanding h-BN aerogel, both the metal and carbon based template need to be removed after the deposition of h-BN. This process can be avoided via a substitution process,[97] in which the graphene aerogels can be completely substituted by h-BN directly and the obtained h-BN aerogels maintains the same structure of graphene aerogels down to the nanometer scale.

Besides the CVD route, assembling from liquid dispersion of h-BN flakes is another promising way to fabricate 3D h-BN foams with high yield and low cost.[99–103] Through solid-state ball milling of h-BN and urea powder, the h-BN can be exfoliated to sub-micro flakes and functionalized with amino groups, greatly enhancing its solubility in water with enhanced concentration up to 30 mg ml^{-1}.[100] The h-BN aerogels obtained by cryodrying the colloidal solution show a density of 1.4 mg cm^{-3} and strong blue light emission under ultraviolet excitation.[100] Zeng et. al. developed a polymer assisted cross-linking and freeze-casting strategy to construct h-BN aerogels. The aerogel shows anisotropic microstructure, leading to anisotropic superelasticity, high compressive strength and excellent energy absorption ability. The unique microstructure also endows the aerogels with ultralow dielectric constant and loss.[102] The viscoelasticity, including dynamic viscoelasticity and creep behavior, is also observed in the h-BN aerogel, implying its potential applications in vibration damping and acoustic suppression.[101] Infiltrating the h-BN networks into epoxy matrix can significantly improve the thermal conductivity and glass transition temperature of the polymer, showing potential applications as thermal interface materials.[103]

Porous h-BN architecture was also synthesized directly through high temperature treatment of mixture of boron and nitrogen sources. The boron source can be boron trioxide, and the nitrogen source can be guanidine hydrochloride and urea.[98,104] The porous h-BN structures obtained through this method show ultrahigh specific surface area from 1152 to

1427 $m^2 g^{-1}$, and low density slightly above 1 mg cm^{-3}, giving rise to excellent sorption performances for a wide range of oils, solvents and dyes.[98,104] Benefiting from its strong resistance to oxidation, the materials with saturated adsorption can be cleaned just by burning in air (Figure 8e–h). The temperature of heat treatment in this method can be reduced from ≈1000 °C to 300 °C by changing the sources to melamine and boric acid.[105] However, the carbon component cannot be completely removed at this low temperature, and the resulting sample is highly carbon doped. Heating mixture of melamine and boric acid at 1000 °C in an ammonia atmosphere can remove the carbonaceous composition, and the obtained h-BN porous material shows the highest specific surface area ever reported for any BN system, up to 1488 $m^2 g^{-1}$, and outstanding hydrogen storage performance.[106] Introducing thiourea as vesicant into the ammonia borane source can improve the reproducibility and yield of 3D h-BN foams, and the obtained foams possess a vesicular structure with hierarchical pores and ultrathin walls.[107]

2.2. Structure and Property Functionalization

2.2.1. Structure and Defects

The h-BN monolayer is a structural analogue of graphene with one sublattice occupied by boron atoms and the other by nitrogen atoms. The sublattice asymmetry of h-BN sheet is manifested as the distinct ionicity of B–N bonds, which is also responsible for a large band gap (5–6 eV) near the Fermi level.[108–110] The combined covalency and ionicity of B–N bonds also account for the piezoelectric and dielectric phenomena in h-BN.[111,112] For multilayer h-BN, there exist six different stacking orders due to the inequivalence of B and N atoms.[113–115] The interlayer interaction between h-BN sheets is dominated by two contributions: the vdW forces for anchoring the layers at a fixed distance and the electrostatic forces for dictating the optimal stacking mode.[115] The energy landscape of bilayer h-BN sheet displays a sliding path of nearly free energy barrier (**Figure 9**a,b).[114,115] Electronic properties of multilayer h-BN depend on the staking mode and layer thickness, to some extent. The band gap of layered h-BN can be effectively modulated by applying external electric field[116–118] or adjusting interlayer distance.[117,119] The external field can sensitively redistribute nearly free-electron states and rapidly reduce the band gap;[118] decreasing interlayer distance could also reduce the band gap,[117] which can be realized through hydrostatic pressure.[119]

In reality, various defects are unavoidable during the production of h-BN, including impurities, vacancies, edges and grain boundaries (GBs). Defects in h-BN have significant influence on the electronic properties,[120–124] photoluminescence,[125] chemical reactivity,[126] mechanical property,[10,127] molecular adsorption and dissociation behaviors of h-BN.[128,129] Thus, insights into the atomic structure of these defects and linkage between the defect structures and their influence on the physical properties are critical.

2.2.1.1. Vacancies and Edges: High-resolution transmission electron microscopy (HRTEM) is the most popular and powerful tool to probe the structure of vacancies and edges of h-BN, because these kinds of defect can be simultaneously introduced under the electron beam irradiation.[28,130–133] These defects was firstly observed by Jin et al. with identification of individual boron and nitrogen atoms.[28] The irradiation induced holes prefer to adopt a triangular shape and are initiated by the formation of boron monovacancies, and the edges of triangle defects are dominant nitrogen terminated zigzag-type (**Figure 10**a–c).[28] The detailed growth process of the triangle defects was further examined by Ryu et al.[133] Combining multiscale atomistic simulations and HRTEM experiments, Kotakoski et al. attributed the formation of boron monovacancies and triangular-shaped multivacancies in h-BN monolayers to the lower knock-on displacement thresholds of B atoms compared to N atoms under the electron irradiation.[132] Different from the reconstruction of vacancy in graphene, no topological defects or vacancy reconstructions were observed in monolayer h-BN, confirming a disfavor of B–B or N–N bonds.[130] However, structural distortions at both the monovacancy and edge h-BN are found in bilayered h-BN.[134,135] A characteristic charge-induced *pm* symmetry configuration was found for boron vacancies, caused by interlayer bond reconstruction across the bilayer h-BN at the negatively charged boron vacancy defects.[134]

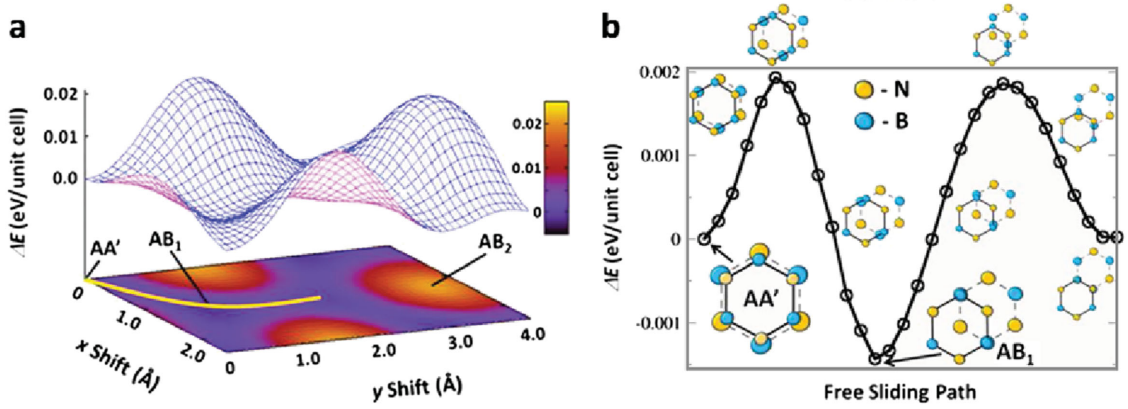

Figure 9. Energy surface (a) and the nearly free-sliding path (b) calculated with respect to the AA' stacking mode. Reproduced with permission.[115] Copyright 2010, American Physical Society.

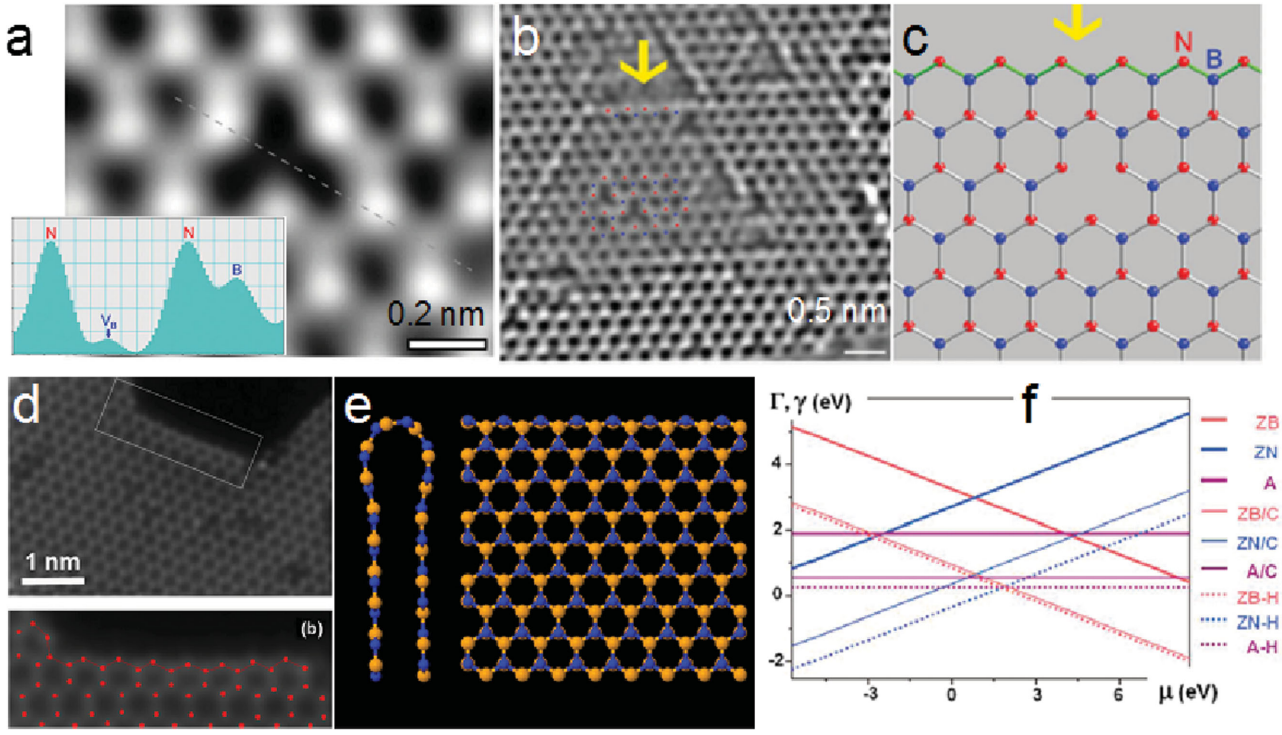

Figure 10. Vacancy and edge structures of h-BN. a) The phase image of reconstructed exit wave of a region containing a boron monovacancy. Insert is the corresponding line profile, confirming the missing atom is boron. b) The phase image of reconstructed exit wave showing the edge is terminated with the nitrogen atoms. c) A model for the edge structure involving two-coordinated nitrogen atoms. Reproduced with permission.[28] Copyright 2009, American Physical Society. d) TEM image indicating structural relaxations at the edge of bilayer h-BN. e) Cross-sectional and plan view schematics of a predicted DFT model showing the formation of interlayer bonds at the zigzag edges of a bilayer h-BN. Reproduced with permission.[135] Copyright 2012, American Physical Society. f) The interface energy as a function of chemical potential of B. Reproduced with permission.[137] Copyright 2011, American Chemical Society.

Covalent interlayer bonds were found to form spontaneously at the edges of a h-BN bilayer, resulting in subangstrom distortions of the edge atomic structure (Figure 10d,e).[135] The closed edge reconstruction makes the material recover its insulating behavior and largely negates the predicted metallic character of open edges.[135] Interlayer bond reconstruction may also be the origination of B terminated zigzag edges and alternating B–N armchair edges observed in multilayer h-BN.[131,136] Although the observed monolayer h-BN edges are dominatingly nitrogen terminated zigzag-type under high vacuum condition in the HRTEM chamber, the edge energy and structures are predicted to depend on the elemental chemical potentials of B and N species, thus the ambient environment (Figure 10f).[137] Besides HRTEM, point defects in h-BN can also be observed and even manipulated by scanning tunneling microscopy (STM) with a top layer of graphene,[138] which provides a conducting drain path for electrical current.

Due to the presence of defect states, vacancies and edges of h-BN will definitely reduce the bandgap of h-BN.[120] Moreover, vacancies in BN can also induce interesting magnetic properties. It has been predicted that the B vacancy defect can induce a spin polarization in the nearest three N atoms while the results on the N vacancy show discrepancies.[120,139,140] The spontaneous magnetization induced by boron vacancy or divacancy can be further switched by biaxial strain.[141]

2.1.1.2. Grain Boundaries: Different from graphene, in which the GBs manifest as a string of pentagon | heptagon dislocations (5|7s) for its lower elastic strain, GBs in h-BN show variability in its dislocation cores. First, the normal 5|7 dislocation has the lowest elastic energy yet the unavoidable homoelemental bonds will raise its chemical energy. In contrast, a square | octagon (4|8) dislocation has higher elastic energy but it could eliminate the homoelemental bonds. Initially, Liu et al. systematically investigated the GBs in h-BN by DFT calculations.[123] They revealed that, depending on the tilt angle of grains, GBs can be either polar (B-rich or N-rich), constituted by 5|7s, or unpolar, composed of 4|8s (**Figure 11**a). The polar GBs carry net charges, positive at B-rich and negative at N-rich ones, giving rise to smaller bandgaps compared to unpolar GBs. These GB structures of h-BN are further observed in CVD deposited h-BN monolayer through HRTEM and STM.[142,143] Migrations of 5|7 GB are also observed,[142] whose mechanisms were suggested as pseudo-climb via atom pair absorption or gliding via Stone-Wales bond rotation.[144] Scanning tunneling spectroscopy also confirmed that the band gap of the 5|7 GB was dramatically decreased as compared with that of the 4|8 GB (Figure 11b–d).[143] Unexpected from the theoretical predication, highly unfavorable polar 4|8 defects with homo-elemental bonds was also produced in a pristine h-BN lattice by electron irradiation at 1000 K.[127] Their migration was observed and

www.MaterialsViews.com

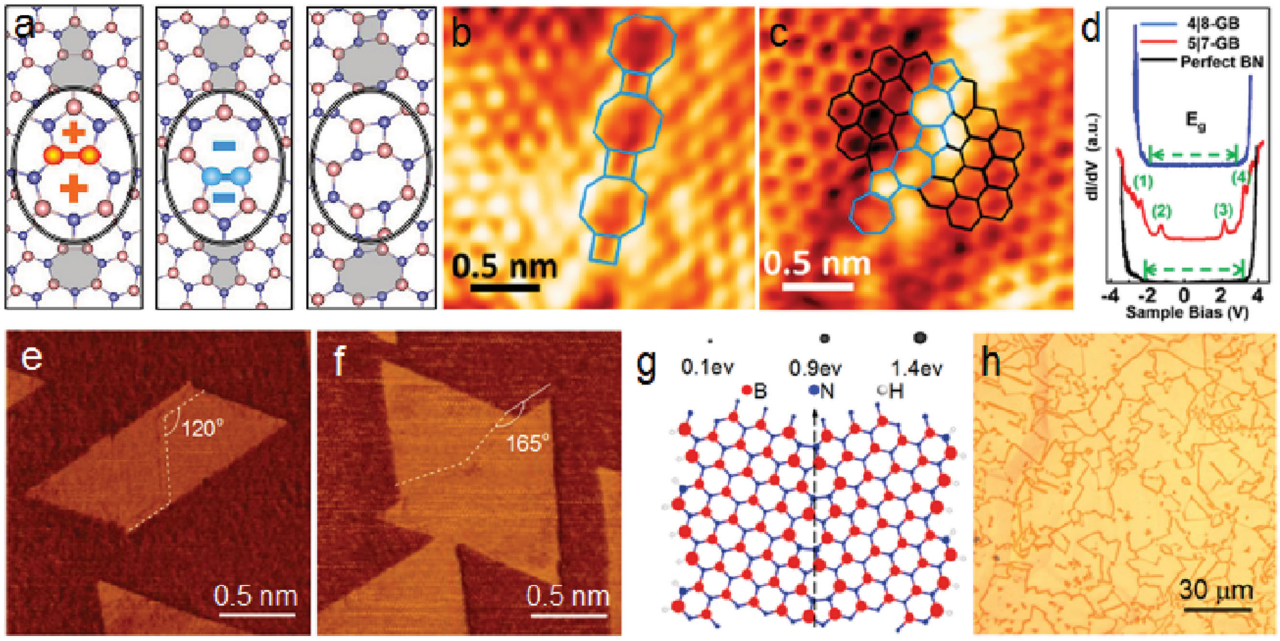

Figure 11. Structure, distribution and etching of h-BN grain boundaries. a) Different types of h-BN grain boundaries predicted by DFT. Reproduced with permission.[123] Copyright 2012, American Chemical Society. b,c) High-resolution STM image of the 4|8 GB (b) and 5|7 GB (c). d) Averaged dI/dV spectra and simulated LDOS of the 4|8 and 5|7 GBs, respectively, using the data from perfect h-BN as reference. Reproduced with permission.[143] Copyright 2015, American Chemical Society. e,f) FFM images of aggregates of h-BN triangles, whose boundary locations are marked by dashed lines. Reproduced with permission.[50] Copyright 2015, Wiley-VCH. g) The model structure with an h-BN boundary. The diameters of the boron and nitrogen atom spheres is proportional to the magnitude of the adsorption energy of a hydrogen atom on top of corresponding boron and nitrogen atoms. h) Optical image of large area h-BN film with etched grain boundaries. Reproduced with permission.[20] Copyright 2015, Wiley-VCH.

explained, which is claimed to be responsible for the plastic deformation of the h-BN layer.[127]

Besides the tilt GBs, GBs stitching two oppositely orientated h-BN domains are also frequently observed in epitaxially grown h-BN.[41,42,50] Although its distribution has been revealed through frictional force microscopy (FFM) (Figure 11e,f) and STM by our group and other groups,[42,50] the corresponding atomic structure has not been explored experimentally. Pentagon-octagon-pentagon (5|8|5), 4|8, and ideal hexagonal structure have all been predicted and investigated through DFT calculations,[50,122,145] and the most stable structure is predicted to strongly depend on the chemical potentials of B and N, related to the synthesis condition.[145]

Another important issue concerning GBs is their distribution over large scale. We recently demonstrated that the GBs of continuous h-BN monolayer film grown on Cu can be precisely etched by hydrogen at elevated temperature.[20] This is attributed to the high reactivity of GBs and edges of openings in h-BN to hydrogen, as confirmed by DFT calculations (Figure 11g). The distribution of the GBs can be then observed by optical microscopy directly with post-annealing in air (Figure 11h), which causes severe oxidization and color change of the exposed Cu surface. Interestingly, the GB are found to be dominantly composed of straight segments at least on the micrometer scale (Figure 11h), in sharp contrast to the widely observed wiggly shaped GBs in graphene. This feature of h-BN GBs shapes should be attributed to the notable dependence of formation energy on the orientation compared to that in elemental 2D materials.[123]

2.2.2. Functionalization

2.2.2.1. Doping by Carbon and Chemical Groups: Chemical doping is an effective approach to control charge carries and magnetic states in h-BN. Located between B and N in periodic table, carbon has a similar atomic size and is very suitable for doping h-BN. The doping states of C atoms embedded in h-BN will be localized in the vicinity of C atoms and extend into the insulating h-BN area. The carbon atoms substituting boron atoms give rise to an unpaired electron and induce a local magnetic moment (**Figure 12**a).[146] Constructing custom-designed C doped h-BN via interaction of CO molecules with vacancy defects in h-BN has been demonstrated theoretically.[147] Besides carbon, transition-metal atoms are also good dopants for h-BN to yield interesting electronic and magnetic properties, which depend on the dopant species (Figure 12b) and are tunable by electric field.[148,149] In particular, embedding Cr, Co and Ni atom can even lead to half-metallic property, which is desired for spin filter applications.[148]

Atomic chemisorption is another effective method for functionalizing h-BN. Fully hydrogenated or fluorinated h-BN sheet can maintain the hexagonal lattice structure with favorable formation energies and reduced band gap.[152] We also found that h-BN on Cu substrate can exhibit ferromagnetic, antiferromagnetic, or ferrimagnetic properties when ozone molecules or oxygen–hydrogen groups are bonded on B atoms (Figure 12c).[150] For multilayer h-BN, intercalating atoms with high and low electronegativities in-between the h-BN layers can induce shallow acceptor and donor states,

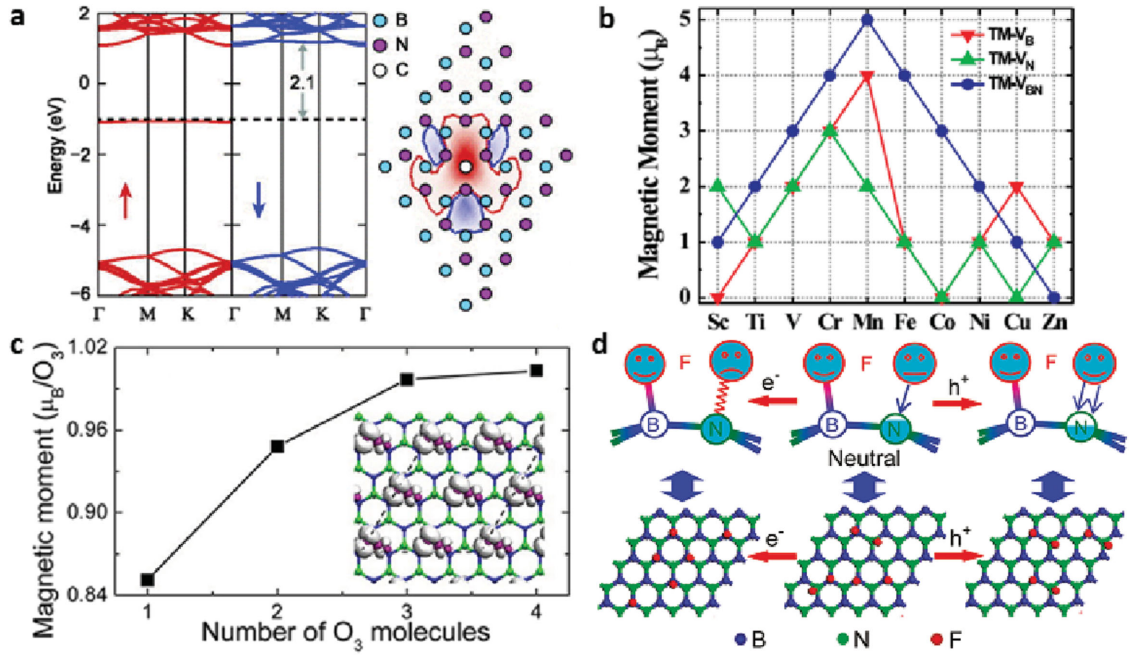

Figure 12. Electrical and magnetic properties of doped h-BN. a) Spin-resolved band structure and spin density plots for single carbon substitution in h-BN. Reproduced with permission.[146] Copyright 2012, American Institute of Physics. b) The magnetic moments of h-BN with transition metal atoms adsorption on boron-vacancy, nitride-vacancy, and boron-nitride-vacancy. Reproduced with permission.[149] Copyright 2012, American Physical Society. c) Total magnetic moment of O_3-functionalized h-BN/Cu as a function of the number of O_3 molecules, which are located at the third adjacent sites. The inset shows the charge density difference for four O_3 molecules in the unit cell with the ferromagnetic state. Reproduced with permission.[150] Copyright 2015, American Chemical Society. d) A schematic diagram for controlling the functionalizations of h-BN by carrier doping. Reproduced with permission.[151] Copyright 2011, American Chemical Society.

respectively.[153] Controlling the functionalization of h-BN is important yet challenging. To this end, a concept of carrier doping to control the functionalizations of h-BN has been proposed by the present authors.[151] When the system is electron-doped, F or H atoms will exclusively bond with B atoms, resulting in possible magnetization of the system, whereas hole doping favors the adatoms to form insulating orthodimer structures on the h-BN structures (Figure 12d).[151]

2.2.2.2. Forming in-plane Hybrid Materials with Graphene: Besides doping, h-BN/graphene (h-BNGR) hybrid materials have also been widely investigated. As the formation energy of h-BNGR significantly decreases with the aggregation of embedded carbon cluster,[154–157] carbon atoms embedded in h-BN prefer to segregate to from graphene quantum dots (GQDs), in consistent with experimental observation.[79] Due to the quantum confinement effects, the embedded GQDs show a notable band gap,[158,159] which is dependent on the shape and size of the GQDs.[159–162] The band gap of embedded GQDs decreases with increase of the GQDs size.[159–162] Further analysis shows that the effective mass of carrier increases exponentially with the distance between GQDs,[159] and the energy states near the Fermi level are strongly localized within and in the vicinity of the GQDs.[158,160–162] Triangular GQDs embedding can induce spin-polarization and lead to intrinsic magnetism.[160–162] Furthermore, the heterogeneous boundary plays an important role in modulating the band gap of systems.[163] The band gap of embedded GQDs is dependent on the excess number of B and N atoms at the boundary,[164] but identical for zigzag and armchair edges.[159]

Besides embedding GQDs, graphene nanoribbons (GNRs) embedded in h-BN have also been investigated. Similar to isolated GNRs, armchair graphene nanoribbons embedded in BN sheets are always semiconductors, while zigzag ones become half-metals with the increase of GNRs width,[155–157,165] giving chance to realize a metal-insulator transition by transverse electric field.[155] The band structure of embedded GNRs is sensitive to their width, rather than the ratio of GNR and h-BN.[166]

2.2.2.3. Vertical vdW Heterostructures: When a graphene sheet is supported on a lattice-matched h-BN substrate, the most stable configuration has one carbon atom on the top of a boron atom with the other one centered above a h-BN ring (**Figure 13**a).[167] The distinct ionicity of h-BN induces the inequivalence of the two carbon sites, leading to a band gap of 0.53 eV,[167] and a smaller electron effective mass and higher carrier mobility than bilayer graphene.[168,169] Applying perpendicular electric field and changing the interlayer distance (Figure 13b) can effectively modulate the band gap.[116,167–169] Monolayer graphene sandwiched between h-BN has also been investigated, and a band gap up to 0.16 eV can be opened simultaneously.[170] Functionalization of h-BN with hydrogen and fluorine can lead to n- or p-type doping of graphene, which may be attributed to the charge transfer between graphene and functionalized h-BN.[171] In practice, due to the 1.8% lattice mismatch and possible misalignment between the two honeycomb lattices, a moiré pattern is present (Figure 13c). For commensurable stacking, the breaking of symmetry causes a periodic local potential, giving

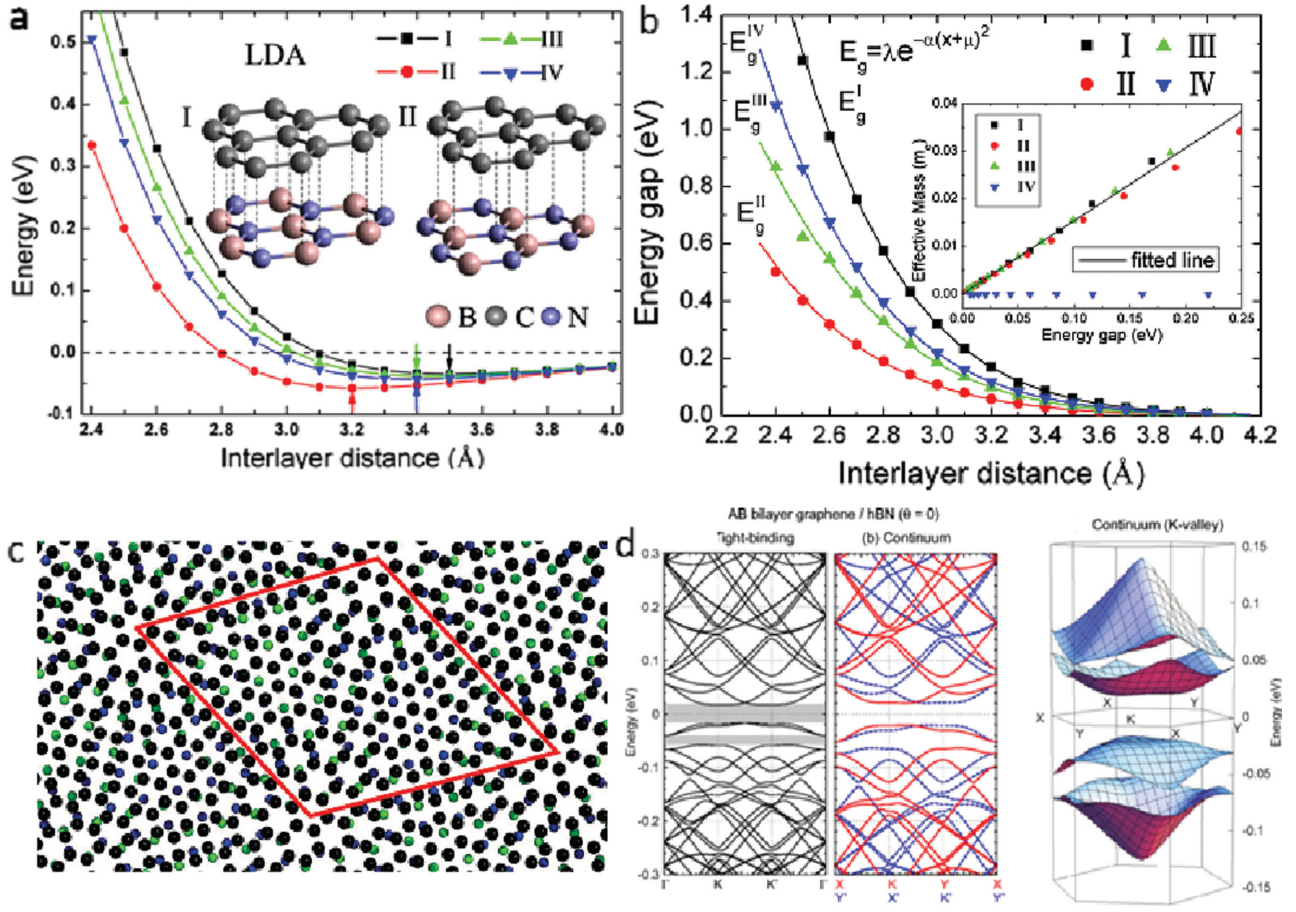

Figure 13. Structure and properties of graphene/h-BN vertical heterostructures. a) Bind energy per unit cell of graphene/h-BN with different stacking patterns as a function of interlayer spacing. b) Variation in the energy gap of graphene/h-BN as a function of interlayer spacing. The inset shows the variation of the effective masses vs band gap. Reproduced with permission.[168] Copyright 2011, American Institute of Physics. c) Two-layer system made of graphene (top layer) and h-BN (bottom layer) with a lattice mismatch. Reproduced with permission.[175] Copyright 2012, American Physical Society. d) Band structures of AB-bilayer graphene/h-BN system and the three-dimensional plot of the first and second electron and hole bands of K-valley. Reproduced with permission.[176] Copyright 2014, American Physical Society.

to a band gap (Figure 13d).[172–177] The induced bandgap can be tuned by the moiré superlattice periodicity, the twist angle and gate voltage. [173,175] However, incommensurable stacking results in a nearly complete close of these gaps, which can be reopened via modulating the separation between graphene and h-BN.[174,178] Due to the incommensuration effects, the Coulomb interaction can lead to spontaneous formation of chiral loop currents in bulk and macroscopic spin-valley order at zero temperature.[179] In the aspect of spin-based devices, h-BN has been proposed to be used as ultimate thick spacers in transition-metal-based magnetoresistive junctions, which shows low resistance area products and typical giant magnetoresistance behavior with magnetoresistive ratios exceeding 100% for certain composition.[180]

2.2.2.4. Phase Transition from h-BN: Cubic boron nitride (c-BN) possesses a number of extreme properties comparable to those of diamond. The present authors demonstrated that, due to strong built-in electric polarization, c-BN (111) nanofilms can be intrinsically metallic and even turn into semiconductors once the thickness is less than 0.69 nm, in sharp contrast to its bulk counterpart (**Figure 14**a).[181] The band gap and dipole moment of the nanofilms can be further significantly tuned by applying an in-plane strain. However, direct synthesis of c-BN with uniform thickness and controllable properties is still a challenging task. The phase transition between different allotropes of BN may provide an alternative route to form c-BN based functional materials. Traditionally, transition from h-BN to c-BN requires a high temperature and pressure.[182] Direct transformation between h-BN and c-BN by pressure is far less favorable than indirect transformation that occurs with the wurtzite BN (w-BN) or rhombic BN (r-BN) as intermediate states, as supported by direct compression simulations (Figure 14b).[183] Recently, a simple chemical synthetic strategy is proposed by the present authors, who found that surface fluorination of few-layered h-BN sheets can produce thermodynamically favorable F-terminated c-BN nanofilms with an embedded N–N bond layer and strong inbuilt electric polarization (Figure 14c). The produced fluorinated c-BN nanofilms have controllable band gap by thickness or inbuilt and applied electric fields. Furthermore, by electron doping at reasonable levels, the nanofilms can even exhibit substantial ferromagnetism.[184]

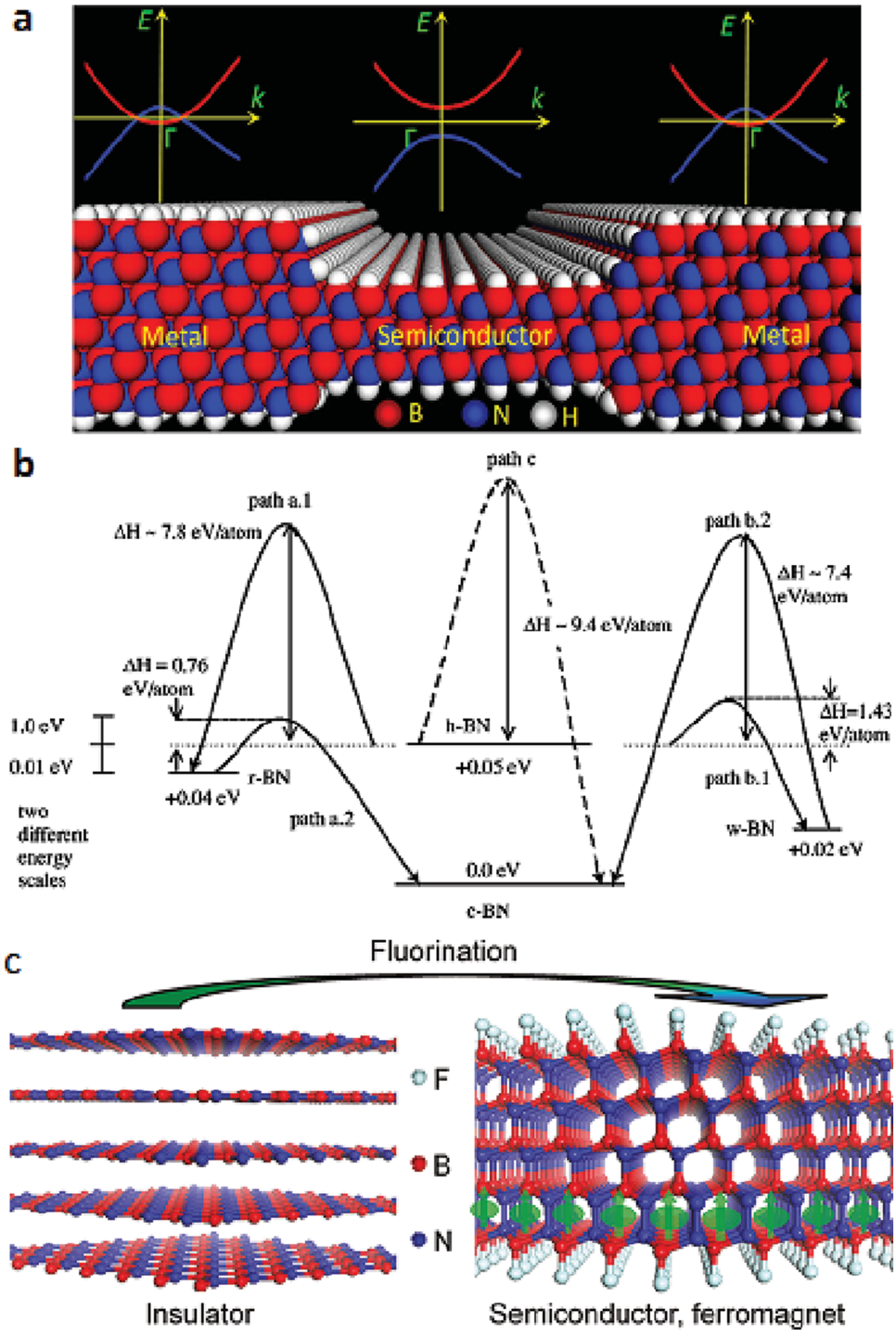

Figure 14. Functions and fabrication of c-BN nanofilm. a) Thickness dependent electrical behavior of c-BN nanofilms. Reproduced with permission.[181] Copyright 2012, American Chemical Society. b) Summary of the energy barriers of various paths in the phase transformations among c-BN, r-BN, h-BN, and w-BN. Reproduced with permission.[183] Copyright 2012, American Physical Society. c) A schematic diagram for the transformation from few-layered h-BN sheets to thermodynamically favorable F-terminated c-BN nanofilms via surface fluorination. Reproduced with permission.[184] Copyright 2011, American Chemical Society.

2.3. Applications of 2D h-BN

Inheriting from bulk h-BN, 2D h-BN possesses various advantageous properties, including excellent stability, high thermal conductivity, electrical insulation, high elastic modulus and low friction coefficient, promising a rich variety of applications. Many applications utilizing the electronic, optical, thermal, mechanical and wetting properties of 2D h-BN have been well summarized previously.[4] In this section, an overview of emerging applications of 2D h-BN is presented.

Among various applications of 2D h-BN explored recently, the most attractive one is constructing vdW heterostructures.

Generally, the h-BN stacked with other 2D materials mainly serves as substrate or ultrathin tunneling barrier. The atomically smooth surface without dangling bonds and charge traps makes h-BN an ideal substrates.[62] In contrast to atomically flat layered oxides of hydrophilic surfaces, on which the mobility of graphene is exceptionally low around 1000 $cm^2 V^{-1} s^{-1}$, a self-cleansing process was observed for h-BN substrates, ensuring an atomically clean interface and graphene mobility up to 500 000 $cm^2 V^{-1} s^{-1}$.[185] Channel materials, including graphene, black phosphorus and TMDCs, supported on or encapsulated between h-BN sheets show intrinsic outstanding performances without notable electron scattering centers.[63,186,187] **Figure 15** compares the mobility of exfoliated monolayer graphene supported on several typical substrates at low temperature (<20 K), highlighting the outstanding performance of h-BN in this aspect.[62,63,185,188–193] Ultrathin h-BN flakes with desired atomically thin thickness enable the construction of devices with novel functions.[64,194,195] Furthermore, the interaction between h-BN and other 2D materials when being stacked together promotes the discovery of many novel phenomenon as mentioned above.[35] Advancements in this field have been comprehensively reviewed by Lim et al.[196]

The excellent thermal and chemical stability of h-BN endows it with promising potential for serving as a multifunctional coating material. Even monolayer h-BN nanosheets can sustain up to 850 °C in air,[197] implying applications as atomic thin high-temperature oxidation-resistant coating. Exfoliated h-BN sheets have shown promising oxidation protection for ferromagnetic contacts in spintronic devices and unstable 2D material channel, including black phosphorus, niobium diselenide and so on.[198,199] Recent developments in fabrication of h-BN further make this application become viable in large area. We have demonstrated that, at 200 °C in air, no oxidization is observed for monolayer h-BN covered Cu, in sharp contrast to bare Cu surface.[200] However, due to the presence of defects including vacancies and grain boundaries, covered Cu surface are gradually oxidized at higher temperature. To resolve this problem, thicker h-BN film is used. Liu et al. have grown h-BN film with controlled thickness on Ni foil and then transferred it onto Cu foil.[201] They found that 5 nm h-BN coating can protect the Cu surface at 500 °C for more than 30 min. For Ni substrate, the temperature is even up to 1100 °C (**Figure 16**a,b). In addition, we showed that monolayer h-BN grown on Cu surface can significantly reduces the friction force of Cu surface by more than 40 fold in a wide range of normal load (Figure 16c).[200] The large band gap of h-BN film makes it also an ideal insulating coating with atomic thickness (Figure 16d).[61,200,202]

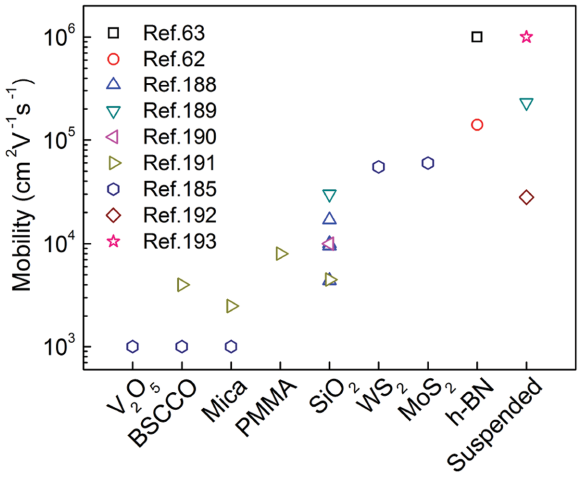

Figure 15. Carrier mobility of exfoliated monolayer graphene supported on several typical substrates at low temperatures (1.7 K – 20 K). The values presented here are the highest magnitude reported in each reference.

When being incorporated into polymer matrixes, h-BN can not only improve the mechanical and thermal performance of the polymer,[203] but also demonstrates versatile functions. Husain et al. demonstrated that h-BN/polyvinyl alcohol coating on stainless steel exhibited improved corrosion resistance under simulated marine environment.[204] h-BN coated or incorporated polymer also shows enhanced oxygen-atom corrosion resistance, which is required for spacecraft in the low earth orbit.[205–208] Barrier and bonding effects of the h-BN nanosheets are responsible for the oxygen-atom protective performance.[207,208] Furthermore, since B is a well-known efficient neutron absorber with a very high neutron-capture cross section, h-BN filled composites[13] are expected to exhibit a good shielding effect against space radiation,[209,210] showing promising potential applications in spacecraft.

As a wide band gap semiconductor with ultraviolet luminescence, h-BN has been proposed as photon emission,[211,212] ultraviolet lasing,[213,214] and deep ultraviolet (DUV) detector.[56,215] DUV detector based on monolayer h-BN has been demonstrated (**Figure 17**a).[216] The charge current is significantly increased by three orders of magnitude when the device is illuminated by a DUV deuterium lamp. Moreover, being an anisotropic media where the principal components of the dielectric tensor have opposite signs, polar h-BN could support hyperbolic phonon-polariton modes.[217] As shown in Figure 17b, it could be utilized as low-loss, mid-infrared and natural hyperbolic material in near-field imaging and sub-diffractional focusing.[218] Besides these applications initiated from perfect h-BN lattice, defects in h-BN offer quite different but intriguing phenomenon. Optical excitation of defect transition in h-BN flakes can result in photoinduced doping in graphene/h-BN heterostructures, which enables flexible and repeatable writing and erasing of charge doping in graphene by visible light (Figure 17c).[219] Moreover, ultrabright single-photon emission has been recently observed around 623 nm from localized defects in both h-BN monolayers and multilayers at room temperature (Figure 17d). These polarized emission centers are suggested to serve as room-temperature quantum emitters.[220]

DNA sequencing through graphene nanopores has been studied for the advantages along with the atomically thin wall. Compared with graphene, h-BN may exhibit more remarkable durability and insulating properties in high-ionic-strength solution, and thus is another promising candidate materials. Liu et al. have demonstrated the DNA translocation through h-BN nanopores.[221] The h-BN nanopores showed much higher sensitivity in DNA single-molecule

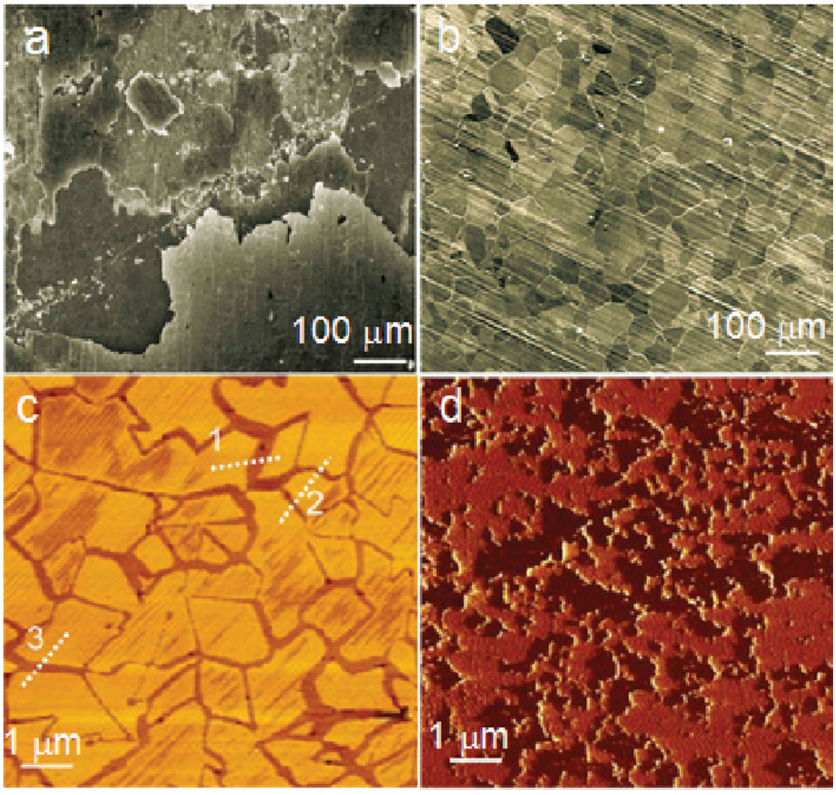

Figure 16. Coating performance of h-BN. a,b) SEM images of pure Ni (a) and 5 nm h-BN-coated Ni foils (b) after oxidization at 1,100 °C. Scale bars, 100 μm. Reproduced with permission.[201] Copyright 2013, Nature Publishing Group. c,d) FFM (c) and current (d) images of partially grown h-BN monolayer on Cu foil. Reproduced with permission.[200] Copyright 2014, IOP Publishing.

detection compared with SiN nanopores, shedding light on applications of h-BN in highly efficient DNA sequencing.

3. Properties and Functionalization of One Dimensional h-BN

3.1. h-BN Nanoribbons

While the 2D h-BN sheet is fundamentally important, their one-dimensional derivatives are more desirable for many applications in devices, especially in current electronics. Like graphene, h-BN can be tailored into 1D nanoribbons along different crystallographic orientations. In contrast to graphene, the binary composition of h-BN endows the h-BN nanoribbons (BNNRs) with more colorful edges, resulting in many exotic properties that depend on the edge composition and chemical passivation. In this section, we review the current progress on the fabrication of BNNRs and their tunable functionality.

3.1.1. Fabrication

The experimental probe of the properties of BNNRs has been severely delayed, because the synthesis of BNNRs is challenging. Chemical vapor deposition has achieved great success in the growth of large area h-BN monolayer, and also shows potential in the fabrication of BNNRs. Simply by cutting off the precursor at the end of the CVD growth, we showed that the h-BN monolayer could be tailored into BNNRs by hydrogen etching along two neighboring grain boundaries in parallel.[20] Although the prepared BNNRs through this method are strictly monolayer, the widths of BNNRs are randomly distributed and hardly controlled. Besides the top-down etching, a bottom-up method was also proposed, using graphene edge as template to epitaxially grow BNNRs.[84] In this method, the width of the BNNRs could be simply controlled by adjusting the growth time.

A more direct way to obtain BNNRs is to unfold or flatten h-BN nanotubes (BNNTs), as firstly demonstrated by the present authors.[222] In 2010, we applied Ar plasma to unzip the BNNTs via etching away the exposed top of multiwall BNNTs (**Figure 18**a), whose side and bottom parts were embedded in PMMA.[222] The obtained BNNRs are as narrow as ≈15 nm, and show semiconducting behavior. Another more effective and facile way to unfold the BNNTs is through alkali metal intercalation (Figure 18b). Potassium-interaction or lithium-assisted longitudinal splitting of BNNTs provides high-quality BNNRs with high aspect ratio and straight parallel edges.[223–225] BNNRs can also be obtained through flatting BNNTs. A high-temperature, extended-pressure inductively coupled thermal plasma system has been developed to produce these desired collapsed BNNTs in large scale.[226]

3.1.2. Basic Structural and Electronic Properties

BNNRs can be classified into three types based on the edge orientation, the armchair, zigzag, and other random edges. The BNNRs with standard armchair (A-BNNRs) and zigzag edges (Z-BNNRs) have attracted most research attention (**Figure 19**a). By DFT relaxation, the armchair edge is shown to be comprised of tilted BN dimers due to asymmetrical dangling bonds on the edge B and N atoms; whereas the zigzag edge can be further divided into B- and N-terminated edges, and their different electro-negativities produce a transverse electric polarization across the zigzag BNNRs. The edge energy for the armchair is lower than the average value for the B- and N-terminated zigzag.[137] However, the relative stability of different edges will depend on chemical balance between B and N. In particular, the edges of BNNRs fabricated by unwrapping BNNTs are mostly in zigzag types.[222,223] The hexagons at zigzag edges could reconstruct into pentagon | heptagon (5|7) defects with lower energy, which, albeit including homoelemental B–B and N–N bonds, in part saturate the edge dangling bonds.[227] A-BNNRs are semiconducting, while the Z-BNNRs possess a magnetic ground state with extended spin

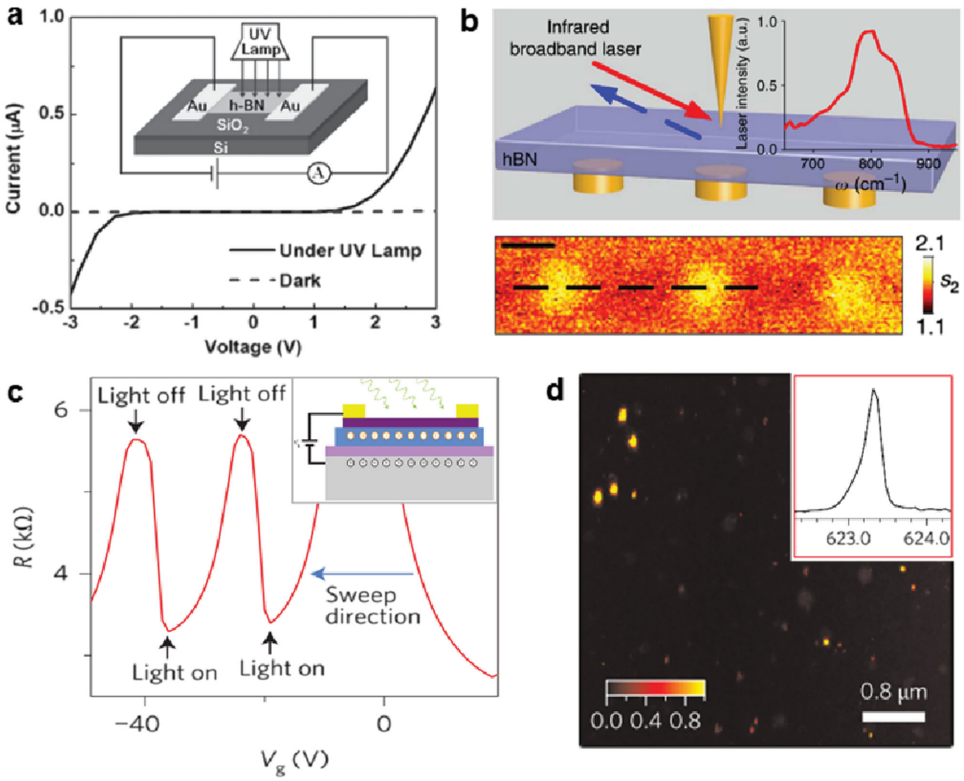

Figure 17. Photoelectrical applications of h-BN. a) I–V characteristics of a DUV detector based on monolayer h-BN in the dark and under a DUV deuterium lamp illumination. Reproduced with permission.[56] Copyright 2015, Wiley-VCH. b) Schematic setup for super-resolution imaging with tunable hyperbolic polaritons. Three gold nanodiscs covered by 150-nm-thick h-BN are displayed by infrared optical amplitude image at bottom. Scale bars, 500 nm. Reproduced with permission.[218] Copyright 2015, Nature Publishing Group. c) Photoinduced doping in graphene/h-BN heterostructures. Graphene resistance R(V_g) is traced with the light illumination alternately switched on and off. Reproduced with permission.[219] Copyright 2014, Nature Publishing Group. d) Scanning confocal map of a multilayer h-BN sample showing bright luminescent spots, some of which correspond to emission from single defects. Inset: the zero phonon line of a defect center taken at 77K. Reproduced with permission.[220] Copyright 2015, Nature Publishing Group.

ordering along the edges.[228] The Z-BNNRs with reconstructed edges become nonmagnetic.[227]

Upon hydrogen passivation, the edge reconstruction of BNNRs is eliminated and they all become nonmagnetic insulators. The present authors showed that the H-terminated Z-BNNR has an indirect bandgap, which decreases with increasing width due to the enhanced spontaneous electric polarization; whereas the H-terminated A-BNNRs have a direct band gap, whose variation versus width exhibits three distinct family behaviors, similar to that present for graphene nanoribbons, resulting from an interplay between quantum confinement effect and bond relaxation at the edges.[229] The H-terminated BNNRs exhibit strong excitonic effect with an exciton binding energy up to 2–3 eV depending on edge direction and ribbon width and a quasiparticle band gap ≈7 eV.[230]

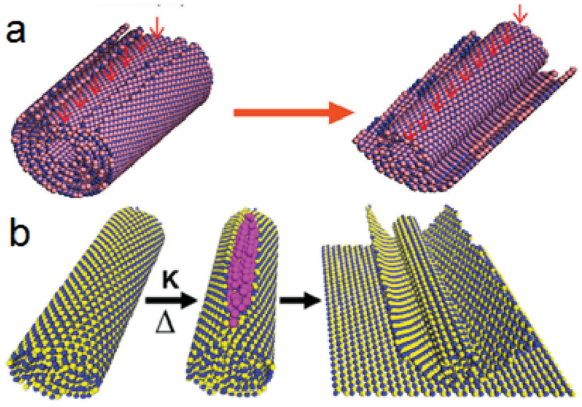

Figure 18. Strategies to fabricate BNNRs. a) Cartoons indicating the top wall domains cutting and their gradual unraveling realized by plasma etching. Reproduced with permission.[222] Copyright 2010, American Chemical Society. b) Schematic of the splitting process of a BNNT to form a BNNR by potassium intercalation. Reproduced with permission.[223] Copyright 2011, American Chemical Society.

3.1.3. Functional Modulation

While BNNRs hold great promise, their wide applications are largely impeded by the electrically insulating properties. To overcome this problem, extensive theoretical efforts have been dedicated to modulating the electronic structures of BNNRs. In the past decade, various strategies for electronic structure modulation have been reported and all can be sorted into three types. The first type is using electronic polarization, produced by either externally applied or built-in electric fields. Applied electric fields can generate a potential difference between the two opposite edges, raising the energy level of valence band maximum at one edge and lowering the level of conduction band minimum at the other

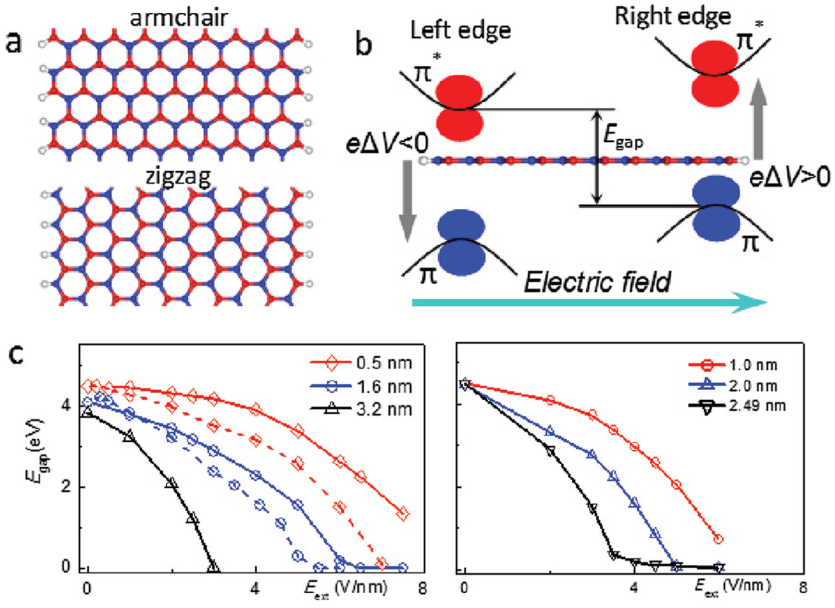

Figure 19. Tunable electronic properties in BN nanoribbons. a) Atomic structures of (upper) armchair and (bottom) zigzag nanoribbons. b) Schematic diagram of the electronic states of a BNNR in the presence of an applied electric field, under which the electrostatic potential on the left edge is lowered while that on the right edge is raised. Correspondingly, the energies of the local π and π^* states at the left edge are decreased and those of the states at the right edge are increased, resulting in band gap reduction. c) Band gap as a function of field strength for the (left) zigzag and (right) armchair nanoribbons of different widths. Dot lines are from the results under reversed electric fields. Reproduced with permission.[229] Copyright 2008, American Physical Society.

(Figure 19b). The as-induced giant Stark effect remarkably changes the band gap of BNNRs, and finally the nearly free electron states, which are weakly bound to the basal h-BN plane and highly sensitive to the perturbation of electrostatic potential, rapidly drop below the Fermi level to metallize the system at sufficiently high field strength.[229] The electric field effect proves to be more remarkable for a wider BNNR (Figure 19c), but the typical field strength required for desirable gap modulation usually reaches the level of V/nm, thereby imposing strict requirements on the corresponding devices. Recently, the present authors showed that that z-BNNRs can be side-by-side assembled into supernanoribbon via considerable hydrogen bonding at interfaces, where the strong interface polarization sharply narrows the band gap of the system to be almost closed with increasing number of component ribbons.[231] This novel strategy for band gap modulation offers unique opportunities for promoting applications of BNNRs in electronic and optical devices. Bare BNNRs exhibit richer electric field effect, including novel field-induced magnetic metal-semiconductor-half-metal transitions and even possible half-metallic Dirac points.[232,233]

The second type is to introduce impurity states into the BNNRs by either chemical decoration at the edges or defect engineering. The impurity states can effectively narrow the band gap and even result in doping effect, which greatly improve the electric transport through the BNNRs. A plenty of theoretical works have been carried out in this aspect, mostly on the z-BNNRs. The z-BNNRs are predicted to become metallic independent of ribbon width when the edges are terminated by oxygen or sulfur atoms.[234] Magnetic and half-metallic properties can also be induced by passivating only the B edge of bare z-BNNRs or partially hydrogenating H-terminated z-BNNRs.[235,236] However, manufacturing these functionalized BNNRs still requires delicate fabrication processes which render the demand for mass production impractical. Later on, efficient electronic and magnetic modulation of z-BNNRs were demonstrated by partial hydrogenation or embedding line defects;[122,124] yet precise control of the structures of passivation interfaces or line defects remains unsettled. Note that even though the impurity states can enhance density of state near the Fermi level, they are often highly localized and will serve as trap states detrimental to carrier transport. Because of these issues, the experimental progress in this field is very limited.

The third type is through strain engineering. The bandgap of both A- and Z-BNNRs can be significantly modulated by applying uniaxial strain,[237,238] which is a general behavior for nanoscale materials. A special point is that the spontaneous polarization in Z-BNNRs can strongly couple to elastic strain, causing not only more remarkable bandgap modulation in wider nanoribbons but also piezoelectric effect.[237] The strain modulation does not produce any localized states or reactive sites in the BNNRs, thus enabling a stable operation in ambient condition. In addition, BNNRs ware predicted to possess ballistic thermoelectric properties superior to graphene nanoribbons due to higher power factor and smaller thermal conductance.[239]

3.2. h-BN Nanotubes

The h-BN sheet can also be wrapped into a seamless cylinder, forming BNNTs, an isostructural analogue to carbon nanotubes. The BNNTs have also been a subject of extensive study owing to their excellent mechanical, electronic and optical properties. First, the mechanical property of BNNTs is featured by its high Young's modulus of ≈0.7 TPa and superb yield strength.[240–242] The zigzag BNNTs can exhibit an axial deformation up to 1% under applied external electric field of 10 V nm^{-1} due to both the converse piezoelectric effect and the electrostrictive effect.[243] Yet the BNNTs are radically flexible and may collapse against interaction with substrates. Second, the BNNTs inherit the insulating property of h-BN sheet and normally have a band gap ≈5.5 eV, independent of tube chirality.[244] This determines that the BNNTs can be a unique optical material for ultraviolet emission. Indeed, strong luminescence in the ultraviolet range has been revealed in BNNTs through cathodoluminescence and photoluminescence.[245,246] Third, most BNNTs are found to

be in zigzag type, as evidenced by the preferred alignment of tube axes along the (1010) direction of a h-BN sheet.[247] When the diameter of zigzag BNNTs is less than 0.95 nm, its bandgap dramatically decreases with decreasing diameter as a result of strong rehybridization effect (**Figure 20**a,b).[248–250] Actually, the smallest BNNT expected to be stable over room temperature is down to (3,0) with a diameter of 0.3 nm,[250] at which the band gap has been reduced to ≈2.0 eV and exciton binding energy increases to ≈3.0 eV, from 0.7 eV in the h-BN sheet.[251] Similar to the BNNR, the BNNT has its electronic structures amenable to effective modulation by means of axial and radial strains, applied transverse electric fields and chemical functionalizations as well.[252,253] In particular, it has been reported that fluorination not only enhances the electronic transport through the BNNTs but also creates substantial ferromagnetic ordering along the nanotubes.[254,255]

The experimentally produced BNNTs tends to be multiwalled and most of them have even number of tube walls.[257] The interwall interaction has significant impact on the electronic properties of multiwalled BNNTs. It is found that the bandgap of a multiwalled BNNT is found to be remarkably lower than any of its single-walled components, attributed to an interwall direct bandgap transition.[258] If the double-walled BNNT is regarded as a coaxial semiconductor junction, then the band alignment between inner and outer walls can be identified to be type II, which can be tuned into type I by squashing the BNNT; meanwhile, the bandgap of a squashed double-walled BNNT can be greatly reduced with a direct-indirect transition.[259] In small double-walled BNNTs, the band gap of the inner wall is distinctly smaller than that of the insulating outer wall so that electron carriers will entirely go to the inner wall, rendering the system a homogeneous nanocable (Figure 20c,d).[256] Such concept was proposed by the present authors and possible to break the tradition of heterogeneous coaxial structures for various cables.

4. Novel B/N Structures and Nanomaterials

4.1. BN Superstructures

Currently identified 3D BN phases are all insulating including c-BN,[260] w-BN,[182] h-BN,[222] and r-BN.[261] Because of the wide band gap,[262] the practical applications of present 3D BN in electronic devices is hindered. With the development of computational technology, various 3D BN superstructures with semiconducting and metallic characters have been predicted by first-principles calculations (**Figure 21**). 3D BN networks containing only sp^2 hybrid B-N bond exhibits semiconducting properties.[263] When 3D BN superstructures are partially hybrid by sp^2 and sp^3 bonds, typically like the predicted tetragonal T-B_nN_n with space group $P\bar{4}m2$, the structure becomes metallic.[264] Though 3D BN phases varying from metal to semiconductor to insulator have been predicted, new forms of 3D BN allotropes with novel properties is still under active investigation. Moreover, experimental fabrication and characterization of these predicted 3D BN phases is a great challenge.

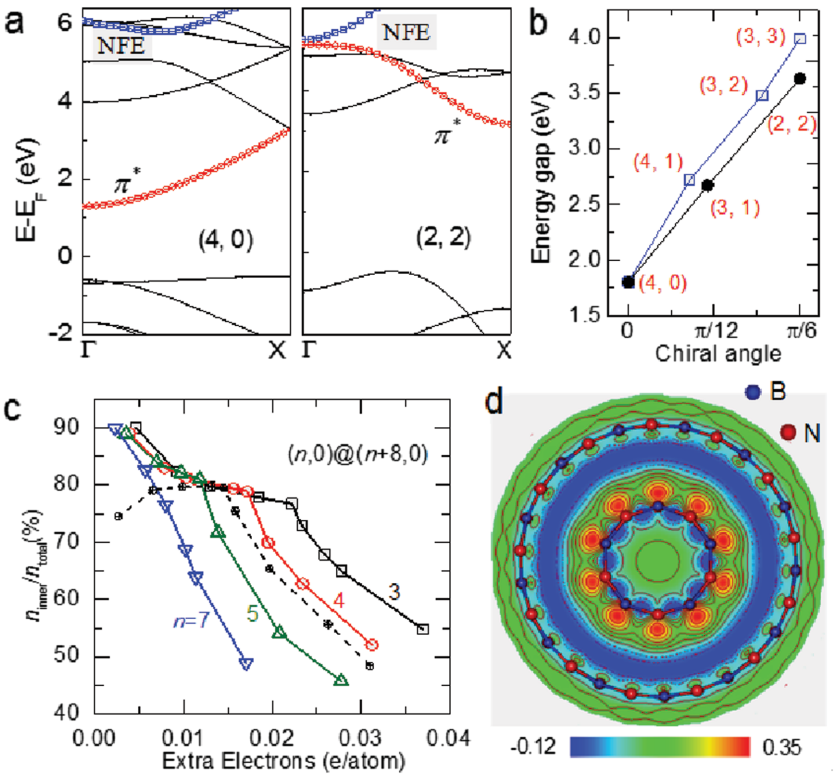

Figure 20. Peculiar electronic properties of small BNNTs. a) Band structures of the (4,0) and (2,2) BNNTs. b) Bandgap of small BNNTs as a function of the chiral angle. Reproduced with permission.[248] Copyright 2009, American Institute of Physics. c) Ratio of charge on the inner wall to total charge in the DBNNT, n_{inner}/n_{total}, for the $(n,0)@(n+8,0)$ double-walled BNNTs (n = 3–7) as a function of charge-injection level. Black dash line is for an ideal case of a (5,0) CNT sheathed in a (14,0) BNNT. (d) Charge density difference in the (5,0)@(13,0) double-walled BNNT at the charge-injection level of 0.07 electrons/atom. Reproduced with permission.[256] Copyright 2010, American Physical Society.

4.2. Novel B/N Nanomaterials

Boron, a nearest neighbor of carbon in the periodic table, is one of the most fascinating elements because of its chemical and structural complexity.[265,266] Boron has a valence electron configuration $2s^22p^1$ and lacks one electron compared to carbon. Boron thus is unable to form stable sp^2 bond hybridization or honeycomb lattice as adopted by graphene. Instead, boron tends to form the so-called multi-center bonding other than the conventional covalent two-electron two-center bonding. Consequently, the research of boron holds a special position in the community of materials chemistry and physics, and exhibits the most diverse polymorphisms.[265,267,268] To date, bulk boron have at least 16 polymorphs such as α-B_{12}, β-B_{106}, T-B_{192} and γ-B_{28} which were prepared usually at high temperature and high pressure.[269–271]

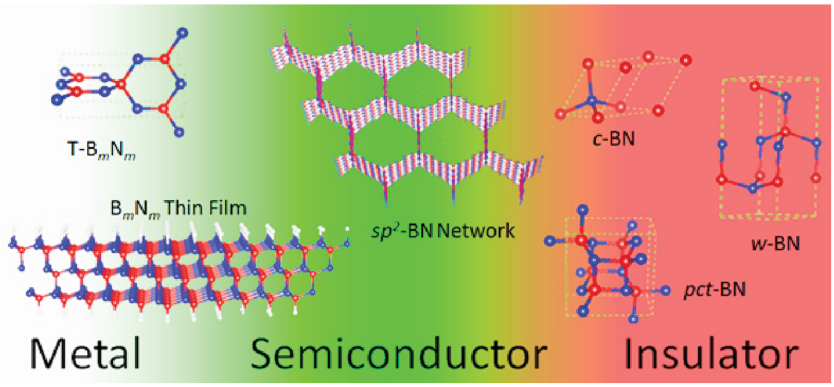

Figure 21. Electronic properties of various BN superstructures from first-principles calculations.

In recent years, extensive theoretical studies have been devoted to investigating possible 2D forms of boron structures, which possess numerous novel structural, electronic, optical, magnetic and thermal properties.[265,266,268,272–276] Apart from bulk (3D) phases,[269,277] 0D fullerences,[278] 1D nanowires,[279–282] nanotubes,[283,284] nanoribbons[285,286] and atomically thin 2D boron films are subjects of extensive study. 2D Boron sheets are usually composed of triangular and hexagonal motifs arising from combination between two- and three-center bonding.[265,276] Polymorphism of monolayer 2D boron have been proposed with different vacancy densities and arrangements.[272,274,276,287–289] A 2D boron nanofilm with *Pmmn* symmetry and finite thickness even exhibits half-metallic nature with distorted Dirac cones,[274] attributed to the hybrid of in-plane p_x and out-of plane p_z states. Very recently, a 2D boron entirely composed of B_{20} clusters in a hexagonal arrangement is predicted to be antiferromagnetic.[290] Experimentally, breakthroughs were just made that boron monolayers of different lattice structures have been grown on the Ag(111) surface by molecular beam epitaxy under ultrahigh vacuum conditions.[291–293] The obtained boron monolayers all show metallic character.

Regrading N-contained 2D materials, non-metal or metal nitrides monolayers have also attracted a lot of attention. The nitride monolayers should have novel electronic and ferromagnetic properties. For instance, Zhang et al. predicted the existence of a monolayer of chromium nitride with ferromagnetism.[294] They revealed the origin of the ferromagnetism arising from p-d exchange interaction between the Cr and N atoms. Meng et al. studied the electronic structure and magnetic properties in a IIIA-nitride monolayer doped with Cu.[295] Their results indicates that the ground state magnetism is mainly determined by the competition between the ferromagnetic p-p/p-d hybridization interaction and the anti-ferromagnetic super-exchange interaction, and the magnetism can be tuned using external strain.

5. Conclusion and Outlook

To date, various synthetic methods for 2D h-BN film have been developed. Generally, the synthesis of monolayer h-BN through CVD has undergone rapid progress and enabled controlled fabrication of domains with large grain size and aligned orientations. It is optimistic that wafer-scale monolayered h-BN single crystal will be realized in the near future. For applications as substrates and dielectric layers of high performance, multilayer h-BN film of high quality and uniformity is required, but its fabrication remains challenging, and new synthetic routes are required to be developed. Once across this hurdle, direct growth of large area vdW heterostructures, especially vertical stacked layers, can be expected. The 3D h-BN architectures have shown promising applications in removal of organic pollutants. However, applications such as high temperature catalysis require to combine with other functional materials and to modulate the assemble structures of 3D h-BN.

Theoretically, BN nanostructures, including 2D h-BN nanosheets, 1D BNNTs and BNNRs, have shown various appealing electrical and magnetic properties via various functionalizing strategies. However, a large gap between the theoretical prediction and experimental realization of these modulation prevents the realization of full potential of BN structures in functional applications. Innovation strategies for further improving the structural design of BN structures and optimizing their electronic modulations remain to be developed.

Several BN superstructures have been predicted with fascinating properties. However, experimental realization of these predicted structure calls upon great efforts from both theoretical and experimental researchers. The emergence of novel B/N nanomaterials, especially boron monolayers, shows us a new area for future study.

Acknowledgements

This work was supported by 973 program (2013CB932604, 2012CB933403), National Natural Science Foundation of China (51472117, 51535005, 61474063, 11302100), Jiangsu NSF (SBK2015022205), the Research Fund of State Key Laboratory of Mechanics and Control of Mechanical Structures (0414K01, 0415G02), the NUAA Fundamental Research Funds (NP2015203), the Innovation Fund of NUAA (NE2015102, NE2015104, NS2014006 and NZ2015101), and a Project Funded by the Priority Academic Program Development of Jiangsu Higher Education Institutions.

[1] W. Balmain, *Philos. Mag. Series* **1842**, *21*, 270.
[2] W. Balmain, *J. Prakt. Chem.* **1842**, *27*, 422.
[3] D. Golberg, Y. Bando, Y. Huang, T. Terao, M. Mitome, C. Tang, C. Zhi, *ACS Nano* **2010**, *4*, 2979.
[4] A. Pakdel, Y. Bando, D. Golberg, *Chem. Soc. Rev.* **2014**, *43*, 934.
[5] S. Bernard, P. Miele, *Mater. Today* **2014**, *17*, 443.

[6] J.-H. Park, J. C. Park, S. J. Yun, H. Kim, D. H. Luong, S. M. Kim, S. H. Choi, W. Yang, J. Kong, K. K. Kim, Y. H. Lee, *ACS Nano* **2014**, *8*, 8520.
[7] G. Kim, A. R. Jang, H. Y. Jeong, Z. Lee, D. J. Kang, H. S. Shin, *Nano Lett.* **2013**, *13*, 1834.
[8] Y. Gao, W. Ren, T. Ma, Z. Liu, Y. Zhang, W.-B. Liu, L.-P. Ma, X. Ma, H.-M. Cheng, *ACS Nano* **2013**, *7*, 5199.
[9] K. K. Kim, A. Hsu, X. Jia, S. M. Kim, Y. Shi, M. Hofmann, D. Nezich, J. F. Rodriguez-Nieva, M. Dresselhaus, T. Palacios, J. Kong, *Nano Lett.* **2012**, *12*, 161.
[10] L. Song, L. Ci, H. Lu, P. B. Sorokin, C. Jin, J. Ni, A. G. Kvashnin, D. G. Kvashnin, J. Lou, B. I. Yakobson, P. M. Ajayan, *Nano Lett.* **2010**, *10*, 3209.
[11] K. H. Lee, H.-J. Shin, J. Lee, I.-y. Lee, G.-H. Kim, J.-Y. Choi, S.-W. Kim, *Nano Lett.* **2012**, *12*, 714.
[12] K. K. Kim, A. Hsu, X. Jia, S. M. Kim, Y. Shi, M. Dresselhaus, T. Palacios, J. Kong, *ACS Nano* **2012**, *6*, 8583.
[13] A. Ismach, H. Chou, D. A. Ferrer, Y. Wu, S. McDonnell, H. C. Floresca, A. Covacevich, C. Pope, R. Piner, M. J. Kim, R. M. Wallace, L. Colombo, R. S. Ruoff, *ACS Nano* **2012**, *6*, 6378.
[14] Y. Shi, C. Hamsen, X. Jia, K. K. Kim, A. Reina, M. Hofmann, A. L. Hsu, K. Zhang, H. Li, Z.-Y. Juang, M. S. Dresselhaus, L.-J. Li, J. Kong, *Nano Lett.* **2010**, *10*, 4134.
[15] S. M. Kim, A. Hsu, M. H. Park, S. H. Chae, S. J. Yun, J. S. Lee, D.-H. Cho, W. Fang, C. Lee, T. Palacios, M. Dresselhaus, K. K. Kim, Y. H. Lee, J. Kong, *Nat. Commun.* **2015**, *6*, 8662.
[16] R. V. Gorbachev, I. Riaz, R. R. Nair, R. Jalil, L. Britnell, B. D. Belle, E. W. Hill, K. S. Novoselov, K. Watanabe, T. Taniguchi, A. K. Geim, P. Blake, *Small* **2011**, *7*, 465.
[17] D. Pacilé, J. C. Meyer, Ç. Ö. Girit, A. Zettl, *Appl. Phys. Lett.* **2008**, *92*, 133107.
[18] X. Li, X. Hao, M. Zhao, Y. Wu, J. Yang, Y. Tian, G. Qian, *Adv. Mater.* **2013**, *25*, 2200.
[19] J. N. Coleman, M. Lotya, A. O'Neill, S. D. Bergin, P. J. King, U. Khan, K. Young, A. Gaucher, S. De, R. J. Smith, I. V. Shvets, S. K. Arora, G. Stanton, H.-Y. Kim, K. Lee, G. T. Kim, G. S. Duesberg, T. Hallam, J. J. Boland, J. J. Wang, J. F. Donegan, J. C. Grunlan, G. Moriarty, A. Shmeliov, R. J. Nicholls, J. M. Perkins, E. M. Grieveson, K. Theuwissen, D. W. McComb, P. D. Nellist, V. Nicolosi, *Science* **2011**, *331*, 568.
[20] J. Yin, J. Yu, X. Li, J. Li, J. Zhou, Z. Zhang, W. Guo, *Small* **2015**, *11*, 4497.
[21] X. Song, J. Gao, Y. Nie, T. Gao, J. Sun, D. Ma, Q. Li, Y. Chen, C. Jin, A. Bachmatiuk, M. Rümmeli, F. Ding, Y. Zhang, Z. Liu, *Nano Res.* **2015**, *8*, 3164.
[22] G. Ning, W. Jinquan, F. Lili, J. Yi, L. Dayao, Z. Hongwei, W. Kunlin, W. Dehai, *Nanotechnology* **2012**, *23*, 415605.
[23] R. Y. Tay, M. H. Griep, G. Mallick, S. H. Tsang, R. S. Singh, T. Tumlin, E. H. T. Teo, S. P. Karna, *Nano Lett.* **2014**, *14*, 839.
[24] L. Wang, B. Wu, J. Chen, H. Liu, P. Hu, Y. Liu, *Adv. Mater.* **2014**, *26*, 1559.
[25] S. Caneva, R. S. Weatherup, B. C. Bayer, B. Brennan, S. J. Spencer, K. Mingard, A. Cabrero-Vilatela, C. Baehtz, A. J. Pollard, S. Hofmann, *Nano Lett.* **2015**, *15*, 1867.
[26] Y. Hao, M. S. Bharathi, L. Wang, Y. Liu, H. Chen, S. Nie, X. Wang, H. Chou, C. Tan, B. Fallahazad, H. Ramanarayan, C. W. Magnuson, E. Tutuc, B. I. Yakobson, K. F. McCarty, Y.-W. Zhang, P. Kim, J. Hone, L. Colombo, R. S. Ruoff, *Science* **2013**, *342*, 720.
[27] G. Lu, T. Wu, Q. Yuan, H. Wang, H. Wang, F. Ding, X. Xie, M. Jiang, *Nat. Commun.* **2015**, *6*, 6160.
[28] C. Jin, F. Lin, K. Suenaga, S. Iijima, *Phys. Rev. Lett.* **2009**, *102*, 195505.
[29] Q. Wu, J.-H. Park, S. Park, S. J. Jung, H. Suh, N. Park, W. Wongwiriyapan, S. Lee, Y. H. Lee, Y. J. Song, *Sci. Rep.* **2015**, *5*, 16159.
[30] Y. Stehle, H. M. Meyer, R. R. Unocic, M. Kidder, G. Polizos, P. G. Datskos, R. Jackson, S. N. Smirnov, I. V. Vlassiouk, *Chem. Mater.* **2015**, *27*, 8041.
[31] R. Y. Tay, H. J. Park, G. H. Ryu, D. Tan, S. H. Tsang, H. Li, W. Liu, E. H. T. Teo, Z. Lee, Y. Lifshitz, R. S. Ruoff, *Nanoscale* **2016**, *8*, 2434.
[32] P. Sutter, J. Lahiri, P. Albrecht, E. Sutter, *ACS Nano* **2011**, *5*, 7303.
[33] Z. Zhang, Y. Liu, Y. Yang, B. I. Yakobson, *Nano Lett.* **2016**, *16*, 1398.
[34] R. Zhao, J. Gao, Z. Liu, F. Ding, *Nanoscale* **2015**, *7*, 9723.
[35] C. R. Dean, L. Wang, P. Maher, C. Forsythe, F. Ghahari, Y. Gao, J. Katoch, M. Ishigami, P. Moon, M. Koshino, T. Taniguchi, K. Watanabe, K. L. Shepard, J. Hone, P. Kim, *Nature* **2013**, *497*, 598.
[36] C. R. Woods, L. Britnell, A. Eckmann, R. S. Ma, J. C. Lu, H. M. Guo, X. Lin, G. L. Yu, Y. Cao, R. V. Gorbachev, A. V. Kretinin, J. Park, L. A. Ponomarenko, M. I. Katsnelson, Y. N. Gornostyrev, K. Watanabe, T. Taniguchi, C. Casiraghi, H. J. Gao, A. K. Geim, K. S. Novoselov, *Nat. Phys.* **2014**, *10*, 451.
[37] A. Nagashima, N. Tejima, Y. Gamou, T. Kawai, C. Oshima, *Phys. Rev. Lett.* **1995**, *75*, 3918.
[38] A. Nagashima, N. Tejima, Y. Gamou, T. Kawai, C. Oshima, *Phys. Rev. B* **1995**, *51*, 4606.
[39] E. Rokuta, Y. Hasegawa, K. Suzuki, Y. Gamou, C. Oshima, A. Nagashima, *Phys. Rev. Lett.* **1997**, *79*, 4609.
[40] G. B. Grad, P. Blaha, K. Schwarz, W. Auwärter, T. Greber, *Phys. Rev. B* **2003**, *68*, 085404.
[41] W. Auwärter, H. U. Suter, H. Sachdev, T. Greber, *Chem. Mater.* **2004**, *16*, 343.
[42] W. Auwärter, M. Muntwiler, J. Osterwalder, T. Greber, *Surf. Sci.* **2003**, *545*, L735.
[43] F. Orlando, P. Lacovig, L. Omiciuolo, N. G. Apostol, R. Larciprete, A. Baraldi, S. Lizzit, *ACS Nano* **2014**, *8*, 12063.
[44] G. Dong, E. B. Fourré, F. C. Tabak, J. W. M. Frenken, *Phys. Rev. Lett.* **2010**, *104*, 096102.
[45] L. Camilli, E. Sutter, P. Sutter, *2D Mater.* **2014**, *1*, 025003.
[46] A. Nagashima, N. Tejima, Y. Gamou, T. Kawai, C. Oshima, *Surf. Sci.* **1996**, *357–358*, 307.
[47] F. Müller, K. Stöwe, H. Sachdev, *Chem. Mater.* **2005**, *17*, 3464.
[48] M. Morscher, M. Corso, T. Greber, J. Osterwalder, *Surf. Sci.* **2006**, *600*, 3280.
[49] F. Müller, S. Hüfner, H. Sachdev, R. Laskowski, P. Blaha, K. Schwarz, *Phys. Rev. B* **2010**, *82*, 113406.
[50] J. Yin, X. Liu, W. Lu, J. Li, Y. Cao, Y. Li, Y. Xu, X. Li, J. Zhou, C. Jin, W. Guo, *Small* **2015**, *11*, 5375.
[51] L. Brown, E. B. Lochocki, J. Avila, C.-J. Kim, Y. Ogawa, R. W. Havener, D.-K. Kim, E. J. Monkman, D. E. Shai, H. I. Wei, M. P. Levendorf, M. Asensio, K. M. Shen, J. Park, *Nano Lett.* **2014**, *14*, 5706.
[52] X. Li, W. Cai, J. An, S. Kim, J. Nah, D. Yang, R. Piner, A. Velamakanni, I. Jung, E. Tutuc, S. K. Banerjee, L. Colombo, R. S. Ruoff, *Science* **2009**, *324*, 1312.
[53] M. H. Khan, Z. Huang, F. Xiao, G. Casillas, Z. Chen, P. J. Molino, H. K. Liu, *Sci. Rep.* **2015**, *5*, 7743.
[54] P. R. Kidambi, R. Blume, J. Kling, J. B. Wagner, C. Baehtz, R. S. Weatherup, R. Schloegl, B. C. Bayer, S. Hofmann, *Chem. Mater.* **2014**, *26*, 6380.
[55] H. Wang, X. Zhang, J. Meng, Z. Yin, X. Liu, Y. Zhao, L. Zhang, *Small* **2015**, *11*, 1542.
[56] H. Wang, X. Zhang, H. Liu, Z. Yin, J. Meng, J. Xia, X.-M. Meng, J. Wu, J. You, *Adv. Mater.* **2015**, *27*, 8109.
[57] Y. Kubota, K. Watanabe, O. Tsuda, T. Taniguchi, *Science* **2007**, *317*, 932.
[58] K. Watanabe, T. Taniguchi, H. Kanda, *Nat. Mater.* **2004**, *3*, 404.
[59] Y. Kubota, K. Watanabe, O. Tsuda, T. Taniguchi, *Chem. Mater.* **2008**, *20*, 1661.
[60] C. Zhang, L. Fu, S. Zhao, Y. Zhou, H. Peng, Z. Liu, *Adv. Mater.* **2014**, *26*, 1776.
[61] P. Sutter, J. Lahiri, P. Zahl, B. Wang, E. Sutter, *Nano Lett.* **2013**, *13*, 276.

[62] C. R. Dean, A. F. Young, I. Meric, C. Lee, L. Wang, S. Sorgenfrei, K. Watanabe, T. Taniguchi, P. Kim, K. L. Shepard, J. Hone, *Nat. Nanotechnol.* **2010**, *5*, 722.
[63] L. Wang, I. Meric, P. Y. Huang, Q. Gao, Y. Gao, H. Tran, T. Taniguchi, K. Watanabe, L. M. Campos, D. A. Muller, J. Guo, P. Kim, J. Hone, K. L. Shepard, C. R. Dean, *Science* **2013**, *342*, 614.
[64] F. Withers, O. Del Pozo-Zamudio, A. Mishchenko, A. P. Rooney, A. Gholinia, K. Watanabe, T. Taniguchi, S. J. Haigh, A. K. Geim, A. I. Tartakovskii, K. S. Novoselov, *Nat. Mater.* **2015**, *14*, 301.
[65] G. Lupina, J. Kitzmann, I. Costina, M. Lukosius, C. Wenger, A. Wolff, S. Vaziri, M. Östling, I. Pasternak, A. Krajewska, W. Strupinski, S. Kataria, A. Gahoi, M. C. Lemme, G. Ruhl, G. Zoth, O. Luxenhofer, W. Mehr, *ACS Nano* **2015**, *9*, 4776.
[66] A. G. F. Garcia, M. Neumann, F. Amet, J. R. Williams, K. Watanabe, T. Taniguchi, D. Goldhaber-Gordon, *Nano Lett.* **2012**, *12*, 4449.
[67] W. Yang, G. Chen, Z. Shi, C.-C. Liu, L. Zhang, G. Xie, M. Cheng, D. Wang, R. Yang, D. Shi, K. Watanabe, T. Taniguchi, Y. Yao, Y. Zhang, G. Zhang, *Nat. Mater.* **2013**, *12*, 792.
[68] S. Tang, H. Wang, Y. Zhang, A. Li, H. Xie, X. Liu, L. Liu, T. Li, F. Huang, X. Xie, M. Jiang, *Sci. Rep.* **2013**, *3*, 2666.
[69] M. Son, H. Lim, M. Hong, H. C. Choi, *Nanoscale* **2011**, *3*, 3089.
[70] S. Tang, H. Wang, H. S. Wang, Q. Sun, X. Zhang, C. Cong, H. Xie, X. Liu, X. Zhou, F. Huang, X. Chen, T. Yu, F. Ding, X. Xie, M. Jiang, *Nat. Commun.* **2015**, *6*, 6499.
[71] S. Roth, F. Matsui, T. Greber, J. Osterwalder, *Nano Lett.* **2013**, *13*, 2668.
[72] M. Wang, S. K. Jang, W.-J. Jang, M. Kim, S.-Y. Park, S.-W. Kim, S.-J. Kahng, J.-Y. Choi, R. S. Ruoff, Y. J. Song, S. Lee, *Adv. Mater.* **2013**, *25*, 2746.
[73] M. Wang, M. Kim, D. Odkhuu, N. Park, J. Lee, W.-J. Jang, S.-J. Kahng, R. S. Ruoff, Y. J. Song, S. Lee, *ACS Nano* **2014**, *8*, 5478.
[74] Z. Liu, L. Song, S. Zhao, J. Huang, L. Ma, J. Zhang, J. Lou, P. M. Ajayan, *Nano Lett.* **2011**, *11*, 2032.
[75] Y.-C. Lin, N. Lu, N. Perea-Lopez, J. Li, Z. Lin, X. Peng, C. H. Lee, C. Sun, L. Calderin, P. N. Browning, M. S. Bresnehan, M. J. Kim, T. S. Mayer, M. Terrones, J. A. Robinson, *ACS Nano* **2014**, *8*, 3715.
[76] J. H. Meng, X. W. Zhang, H. L. Wang, X. B. Ren, C. H. Jin, Z. G. Yin, X. Liu, H. Liu, *Nanoscale* **2015**, *7*, 16046.
[77] C. Zhang, S. Zhao, C. Jin, A. L. Koh, Y. Zhou, W. Xu, Q. Li, Q. Xiong, H. Peng, Z. Liu, *Nat. Commun.* **2015**, *6*, 6519.
[78] X. Ling, Y.-H. Lee, Y. Lin, W. Fang, L. Yu, M. S. Dresselhaus, J. Kong, *Nano Lett.* **2014**, *14*, 464.
[79] L. Ci, L. Song, C. Jin, D. Jariwala, D. Wu, Y. Li, A. Srivastava, Z. F. Wang, K. Storr, L. Balicas, F. Liu, P. M. Ajayan, *Nat. Mater.* **2010**, *9*, 430.
[80] M. P. Levendorf, C.-J. Kim, L. Brown, P. Y. Huang, R. W. Havener, D. A. Muller, J. Park, *Nature* **2012**, *488*, 627.
[81] Z. Liu, L. Ma, G. Shi, W. Zhou, Y. Gong, S. Lei, X. Yang, J. Zhang, J. Yu, K. P. Hackenberg, A. Babakhani, J.-C. Idrobo, R. Vajtai, J. Lou, P. M. Ajayan, *Nat. Nanotech.* **2013**, *8*, 119.
[82] P. Sutter, R. Cortes, J. Lahiri, E. Sutter, *Nano Lett.* **2012**, *12*, 4869.
[83] Y. Gao, Y. Zhang, P. Chen, Y. Li, M. Liu, T. Gao, D. Ma, Y. Chen, Z. Cheng, X. Qiu, W. Duan, Z. Liu, *Nano Lett.* **2013**, *13*, 3439.
[84] G. H. Han, J. A. Rodríguez-Manzo, C.-W. Lee, N. J. Kybert, M. B. Lerner, Z. J. Qi, E. N. Dattoli, A. M. Rappe, M. Drndic, A. T. C. Johnson, *ACS Nano* **2013**, *7*, 10129.
[85] L. Liu, J. Park, D. A. Siegel, K. F. McCarty, K. W. Clark, W. Deng, L. Basile, J. C. Idrobo, A.-P. Li, G. Gu, *Science* **2014**, *343*, 163.
[86] P. Sutter, Y. Huang, E. Sutter, *Nano Lett.* **2014**, *14*, 4846.
[87] Y. Gong, G. Shi, Z. Zhang, W. Zhou, J. Jung, W. Gao, L. Ma, Y. Yang, S. Yang, G. You, R. Vajtai, Q. Xu, A. H. MacDonald, B. I. Yakobson, J. Lou, Z. Liu, P. M. Ajayan, *Nat. Commun.* **2014**, *5*, 3193.
[88] G. Kim, H. Lim, K. Y. Ma, A. R. Jang, G. H. Ryu, M. Jung, H.-J. Shin, Z. Lee, H. S. Shin, *Nano Lett.* **2015**, *15*, 4769.
[89] T. Gao, X. Song, H. Du, Y. Nie, Y. Chen, Q. Ji, J. Sun, Y. Yang, Y. Zhang, Z. Liu, *Nat. Commun.* **2015**, *6*, 6835.
[90] J. Yin, X. Li, J. Zhou, W. Guo, *Nano Lett.* **2013**, *13*, 3232.
[91] Z. Chen, W. Ren, L. Gao, B. Liu, S. Pei, H.-M. Cheng, *Nat. Mater.* **2011**, *10*, 424.
[92] T. A. Schaedler, A. J. Jacobsen, A. Torrents, A. E. Sorensen, J. Lian, J. R. Greer, L. Valdevit, W. B. Carter, *Science* **2011**, *334*, 962.
[93] T. Ashton, A. Moore, *J. Mater. Sci.* **2015**, *50*, 6220.
[94] M. Loeblein, R. Y. Tay, S. H. Tsang, W. B. Ng, E. H. T. Teo, *Small* **2014**, *10*, 2992.
[95] Y. Song, B. Li, S. Yang, G. Ding, C. Zhang, X. Xie, *Sci. Rep.* **2015**, *5*, 10337.
[96] S. Schlienger, J. Alauzun, F. Michaux, L. Vidal, J. Parmentier, C. Gervais, F. Babonneau, S. Bernard, P. Miele, J. B. Parra, *Chem. Mater.* **2012**, *24*, 88.
[97] M. Rousseas, A. P. Goldstein, W. Mickelson, M. A. Worsley, L. Woo, A. Zettl, *ACS Nano* **2013**, *7*, 8540.
[98] W. Lei, D. Portehault, D. Liu, S. Qin, Y. Chen, *Nat. Commun.* **2013**, *4*, 1777.
[99] S. M. Jung, H. Y. Jung, M. S. Dresselhaus, Y. J. Jung, J. Kong, *Sci. Rep.* **2012**, *2*, 849.
[100] W. Lei, V. N. Mochalin, D. Liu, S. Qin, Y. Gogotsi, Y. Chen, *Nat. Commun.* **2015**, *6*, 8849.
[101] X. Zeng, L. Ye, R. Sun, J. Xu, C.-P. Wong, *Phys. Chem. Chem. Phys.* **2015**, *17*, 16709.
[102] X. Zeng, L. Ye, S. Yu, R. Sun, J. Xu, C.-P. Wong, *Chem. Mater.* **2015**, *27*, 5849.
[103] X. Zeng, Y. Yao, Z. Gong, F. Wang, R. Sun, J. Xu, C.-P. Wong, *Small* **2015**, *11*, 6205.
[104] D. Liu, W. Lei, S. Qin, Y. Chen, *Sci. Rep.* **2014**, *4*, 4453.
[105] C. Gautam, C. S. Tiwary, S. Jose, G. Brunetto, S. Ozden, S. Vinod, P. Raghavan, S. Biradar, D. S. Galvao, P. M. Ajayan, *ACS Nano* **2015**, *9*, 12088.
[106] Q. Weng, X. Wang, C. Zhi, Y. Bando, D. Golberg, *ACS Nano* **2013**, *7*, 1558.
[107] H. Zhao, X. Song, H. Zeng, *NPG Asia Mater.* **2015**, *7*, e168.
[108] L. Liu, Y. P. Feng, Z. X. Shen, *Phys. Rev. B* **2003**, *68*, 104102.
[109] A. Zunger, A. Katzir, A. Halperin, *Phys. Rev. B* **1976**, *13*, 5560.
[110] B. Arnaud, S. Lebegue, P. Rabiller, M. Alouani, *Phys. Rev. Lett.* **2006**, *96*, 026402.
[111] K. H. Michel, B. Verberck, *Phys. Rev. B* **2009**, *80*, 224301.
[112] K. H. Michel, B. Verberck, *Phys. Rev. B* **2011**, *83*, 115328.
[113] Y. Qi, L. G. Hector, *Appl. Phys. Lett.* **2007**, *90*, 081922.
[114] G. Constantinescu, A. Kuc, T. Heine, *Phys. Rev. Lett.* **2013**, *111*, 036104.
[115] N. Marom, J. Bernstein, J. Garel, A. Tkatchenko, E. Joselevich, L. Kronik, O. Hod, *Phys. Rev. Lett.* **2010**, *105*, 046801.
[116] R. Balu, X. Zhong, R. Pandey, S. P. Karna, *Appl. Phys. Lett.* **2012**, *100*, 052104.
[117] Z. Yang, J. Ni, *J. Appl. Phys.* **2010**, *107*, 104301.
[118] M. Otani, S. Okada, *Physi. Rev. B* **2011**, *83*, 073405.
[119] M. L. Hu, J. L. Yin, C. X. Zhang, Z. Yu, L. Z. Sun, *J. Appl. Phys.* **2011**, *109*, 073708.
[120] S. Azevedo, J. R. Kaschny, C. M. C. de Castilho, F. de Brito Mota, *Eur. Phys. J. B* **2009**, *67*, 507.
[121] A. K. Geim, I. V. Grigorieva, *Nature* **2013**, *499*, 419.
[122] X. Li, X. Wu, X. C. Zeng, J. Yang, *ACS Nano* **2012**, *6*, 4104.
[123] Y. Liu, X. Zou, B. I. Yakobson, *ACS Nano* **2012**, *6*, 7053.
[124] S. Tang, S. Zhang, *J. Phys. Chem. C* **2013**, *117*, 17309.
[125] L. Museur, E. Feldbach, A. Kanaev, *Phys. Rev. B* **2008**, *78*, 155204.
[126] Y. Lin, T. V. Williams, W. Cao, H. E. Elsayed-Ali, J. W. Connell, *J. Phys. Chem. C* **2010**, *114*, 17434.
[127] O. Cretu, Y.-C. Lin, K. Suenaga, *Nano Lett.* **2014**, *14*, 1064.
[128] Y.-H. Zhang, K.-G. Zhou, X.-C. Gou, K.-F. Xie, H.-L. Zhang, Y. Peng, *Chem. Phys. Lett.* **2010**, *484*, 266.
[129] X. Wu, J. Yang, J. G. Hou, Q. Zhu, *J. Chem. Phys.* **2006**, *124*, 054706.

[130] J. C. Meyer, A. Chuvilin, G. Algara-Siller, J. Biskupek, U. Kaiser, *Nano Lett.* **2009**, *9*, 2683.
[131] N. Alem, R. Erni, C. Kisielowski, M. D. Rossell, W. Gannett, A. Zettl, *Phys. Rev. B* **2009**, *80*, 155425.
[132] J. Kotakoski, C. H. Jin, O. Lehtinen, K. Suenaga, A. V. Krasheninnikov, *Phys. Rev. B* **2010**, *82*, 113404.
[133] G. H. Ryu, H. J. Park, J. Ryou, J. Park, J. Lee, G. Kim, H. S. Shin, C. W. Bielawski, R. S. Ruoff, S. Hong, Z. Lee, *Nanoscale* **2015**, *7*, 10600.
[134] N. Alem, O. V. Yazyev, C. Kisielowski, P. Denes, U. Dahmen, P. Hartel, M. Haider, M. Bischoff, B. Jiang, S. G. Louie, A. Zettl, *Phys. Rev. Lett.* **2011**, *106*, 126102.
[135] N. Alem, Q. M. Ramasse, C. R. Seabourne, O. V. Yazyev, K. Erickson, M. C. Sarahan, C. Kisielowski, A. J. Scott, S. G. Louie, A. Zettl, *Phys. Rev. Lett.* **2012**, *109*, 205502.
[136] J. H. Warner, M. H. Rümmeli, A. Bachmatiuk, B. Büchner, *ACS Nano* **2010**, *4*, 1299.
[137] Y. Liu, S. Bhowmick, B. I. Yakobson, *Nano Lett.* **2011**, *11*, 3113.
[138] D. Wong, J. VelascoJr, L. Ju, J. Lee, S. Kahn, H.-Z. Tsai, C. Germany, T. Taniguchi, K. Watanabe, A. Zettl, F. Wang, M. F. Crommie, *Nat. Nanotechnol.* **2015**, *10*, 949.
[139] J. Yang, D. Kim, J. Hong, X. Qian, *Surf. Sci.* **2010**, *604*, 1603.
[140] M. S. Si, D. S. Xue, *Phys. Rev. B* **2007**, *75*, 193409.
[141] B. Ouyang, J. Song, *Appl. Phys. Lett.* **2013**, *103*, 102401.
[142] A. L. Gibb, N. Alem, J.-H. Chen, K. J. Erickson, J. Ciston, A. Gautam, M. Linck, A. Zettl, *J. Am. Chem. Soc.* **2013**, *135*, 6758.
[143] Q. Li, X. Zou, M. Liu, J. Sun, Y. Gao, Y. Qi, X. Zhou, B. I. Yakobson, Y. Zhang, Z. Liu, *Nano Lett.* **2015**, *15*, 5804.
[144] J. Wang, S. N. Li, J. B. Liu, *J. Phys. Chem. A* **2015**, *119*, 3621.
[145] L. C. Gomes, S. S. Alexandre, H. Chacham, R. W. Nunes, *J. Phys. Chem. C* **2013**, *117*, 11770.
[146] H. Park, A. Wadehra, J. W. Wilkins, A. H. Castro Neto, *Appl. Phys. Lett.* **2012**, *100*, 253115.
[147] Z. Liu, Q. Xue, T. Zhang, Y. Tao, C. Ling, M. Shan, *J. Phys. Chem. C* **2013**, *117*, 9332.
[148] Y. G. Zhou, P. Yang, Z. G. Wang, X. T. Zu, H. Y. Xiao, X. Sun, M. A. Khaleel, F. Gao, *Phys. Chem. Chem. Phys.* **2011**, *13*, 7378.
[149] B. Huang, H. Xiang, J. Yu, S. H. Wei, *Phys. Rev. Lett.* **2012**, *108*, 206802.
[150] Y. Guo, W. Guo, *J. Phys. Chem. C* **2015**, *119*, 873.
[151] Z. Zhang, W. Guo, *J. Phys. Chem. Lett.* **2011**, *2*, 2168.
[152] S. Tang, Z. Cao, *Chem. Phys. Lett.* **2010**, *488*, 67.
[153] F. Oba, A. Togo, I. Tanaka, K. Watanabe, T. Taniguchi, *Phys. Rev. B* **2010**, *81*, 075125.
[154] Y. Liu, S. Bhowmick, B. I. Yakobson, *Nano Lett.* **2011**, *11*, 3113.
[155] S. Bhowmick, A. K. Singh, B. I. Yakobson, *J. Phys. Chem. C* **2011**, *115*, 9889.
[156] S. Jungthawan, S. Limpijumnong, J.-L. Kuo, *Phys. Rev. B* **2011**, *84*, 235424.
[157] Y. Ding, Y. Wang, J. Ni, *Appl. Phys. Lett.* **2009**, *95*, 123105.
[158] J. Li, V. B. Shenoy, *Appl. Phys. Lett.* **2011**, *98*, 013105.
[159] R. Zhao, J. Wang, M. Yang, Z. Liu, Z. Liu, *Phys. Chem. Chem. Phys.* **2013**, *15*, 803.
[160] Y. Zhou, Z. Wang, P. Yang, F. Gao, *J. Phys. Chem. C* **2012**, *116*, 7581.
[161] M. Kan, J. Zhou, Q. Wang, Q. Sun, P. Jena, *Phys. Rev. B* **2011**, *84*, 205412.
[162] A. Ramasubramaniam, D. Naveh, *Phys. Rev. B* **2011**, *84*, 075405.
[163] X. F. Chen, J. S. Lian, Q. Jiang, *Phys. Rev. B* **2012**, *86*, 125437.
[164] J. da Rocha Martins, H. Chacham, *ACS Nano* **2010**, *5*, 385.
[165] A. Y. Liu, R. M. Wentzcovitch, M. L. Cohen, *Phys. Rev. B* **1989**, *39*, 1760.
[166] M. Bernardi, M. Palummo, J. C. Grossman, *Phys. Rev. Lett.* **2012**, *108*, 226805.
[167] G. Giovannetti, P. A. Khomyakov, G. Brocks, P. J. Kelly, J. van den Brink, *Phys. Rev. B* **2007**, *76*, 073103.
[168] Y. Fan, M. Zhao, Z. Wang, X. Zhang, H. Zhang, *Appl. Phys. Lett.* **2011**, *98*, 083103.
[169] J. Sławi ska, I. Zasada, Z. Klusek, *Phys. Rev. B* **2010**, *81*, 155433.
[170] S. Tang, J. Yu, L. Liu, *Phys. Chem. Chem. Phys.* **2013**, *15*, 5067.
[171] R. Quhe, J. Zheng, G. Luo, Q. Liu, R. Qin, J. Zhou, D. Yu, S. Nagase, W.-N. Mei, Z. Gao, J. Lu, *NPG Asia Mater.* **2012**, *4*, e6.
[172] J. Jung, A. M. DaSilva, A. H. MacDonald, S. Adam, *Nat. Commun.* **2015**, *6*, 6308.
[173] J. C. Song, A. V. Shytov, L. S. Levitov, *Phys. Rev. Lett.* **2013**, *111*, 266801.
[174] M. Titov, M. I. Katsnelson, *Phys. Rev. Lett.* **2014**, *113*, 096801.
[175] M. Kindermann, B. Uchoa, D. L. Miller, *Phys. Rev. B* **2012**, *86*, 115415.
[176] P. Moon, M. Koshino, *Phys. Rev. B* **2014**, *90*, 155406.
[177] B. Sachs, T. O. Wehling, M. I. Katsnelson, A. I. Lichtenstein, *Phys. Rev. B* **2011**, *84*, 195414.
[178] M. Bokdam, T. Amlaki, G. Brocks, P. J. Kelly, *Phys. Rev. B* **2014**, *89*, 201404.
[179] B. Uchoa, V. N. Kotov, M. Kindermann, *Phys. Rev. B* **2015**, *91*, 121412.
[180] O. V. Yazyev, A. Pasquarello, *Phys. Rev. B* **2009**, *80*, 035408.
[181] Z. Zhang, W. Guo, *Nano Lett.* **2012**, *12*, 3650.
[182] F. P. Bundy, R. H. Wentorf, *J. Chem. Phys.* **1963**, *38*, 1144.
[183] W. J. Yu, W. M. Lau, S. P. Chan, Z. F. Liu, Q. Q. Zheng, *Phys. Rev. B* **2003**, *67*, 014108.
[184] Z. Zhang, X. C. Zeng, W. Guo, *J. Am. Chem. Soc.* **2011**, *133*, 14831.
[185] A. V. Kretinin, Y. Cao, J. S. Tu, G. L. Yu, R. Jalil, K. S. Novoselov, S. J. Haigh, A. Gholinia, A. Mishchenko, M. Lozada, T. Georgiou, C. R. Woods, F. Withers, P. Blake, G. Eda, A. Wirsig, C. Hucho, K. Watanabe, T. Taniguchi, A. K. Geim, R. V. Gorbachev, *Nano Lett.* **2014**, *14*, 3270.
[186] X. Cui, G.-H. Lee, Y. D. Kim, G. Arefe, P. Y. Huang, C.-H. Lee, D. A. Chenet, X. Zhang, L. Wang, F. Ye, F. Pizzocchero, B. S. Jessen, K. Watanabe, T. Taniguchi, D. A. Muller, T. Low, P. Kim, J. Hone, *Nat. Nanotech.* **2015**, *10*, 534.
[187] L. Li, G. J. Ye, V. Tran, R. Fei, G. Chen, H. Wang, J. Wang, K. Watanabe, T. Taniguchi, L. Yang, X. H. Chen, Y. Zhang, *Nat. Nanotechnol.* **2015**, *10*, 608.
[188] X. Hong, K. Zou, J. Zhu, *Phys. Rev. B* **2009**, *80*, 241415.
[189] K. I. Bolotin, K. J. Sikes, Z. Jiang, M. Klima, G. Fudenberg, J. Hone, P. Kim, H. L. Stormer, *Solid State Commun.* **2008**, *146*, 351.
[190] J.-H. Chen, C. Jang, S. Xiao, M. Ishigami, M. S. Fuhrer, *Nat. Nanotechnol.* **2008**, *3*, 206.
[191] L. A. Ponomarenko, R. Yang, T. M. Mohiuddin, M. I. Katsnelson, K. S. Novoselov, S. V. Morozov, A. A. Zhukov, F. Schedin, E. W. Hill, A. K. Geim, *Phys. Rev. Lett.* **2009**, *102*, 206603.
[192] X. Du, I. Skachko, A. Barker, E. Y. Andrei, *Nat. Nanotechnol.* **2008**, *3*, 491.
[193] E. V. Castro, H. Ochoa, M. I. Katsnelson, R. V. Gorbachev, D. C. Elias, K. S. Novoselov, A. K. Geim, F. Guinea, *Phys. Rev. Lett.* **2010**, *105*, 266601.
[194] L. Britnell, R. V. Gorbachev, R. Jalil, B. D. Belle, F. Schedin, A. Mishchenko, T. Georgiou, M. I. Katsnelson, L. Eaves, S. V. Morozov, N. M. R. Peres, J. Leist, A. K. Geim, K. S. Novoselov, L. A. Ponomarenko, *Science* **2012**, *335*, 947.
[195] R. V. Gorbachev, A. K. Geim, M. I. Katsnelson, K. S. Novoselov, T. Tudorovskiy, I. V. Grigorieva, A. H. MacDonald, S. V. Morozov, K. Watanabe, T. Taniguchi, L. A. Ponomarenko, *Nat. Phys.* **2012**, *8*, 896.
[196] H. Lim, S. I. Yoon, G. Kim, A. R. Jang, H. S. Shin, *Chem. Mater.* **2014**, *26*, 4891.
[197] L. H. Li, J. Cervenka, K. Watanabe, T. Taniguchi, Y. Chen, *ACS Nano* **2014**, *8*, 1457.
[198] S. Zihlmann, P. Makk, C. Vaz, C. Schönenberger, arXiv preprint arXiv:1509.03087 **2015**.
[199] Y. Cao, A. Mishchenko, G. L. Yu, E. Khestanova, A. P. Rooney, E. Prestat, A. V. Kretinin, P. Blake, M. B. Shalom, C. Woods,

J. Chapman, G. Balakrishnan, I. V. Grigorieva, K. S. Novoselov, B. A. Piot, M. Potemski, K. Watanabe, T. Taniguchi, S. J. Haigh, A. K. Geim, R. V. Gorbachev, *Nano Lett.* **2015**, *15*, 4914.
[200] X. Li, J. Yin, J. Zhou, W. Guo, *Nanotechnology* **2014**, *25*, 105701.
[201] Z. Liu, Y. Gong, W. Zhou, L. Ma, J. Yu, J. C. Idrobo, J. Jung, A. H. MacDonald, R. Vajtai, J. Lou, P. M. Ajayan, *Nat. Commun.* **2013**, *4*, 2541.
[202] G.-H. Lee, Y.-J. Yu, C. Lee, C. Dean, K. L. Shepard, P. Kim, J. Hone, *Appl. Phys. Lett.* **2011**, *99*, 243114.
[203] C. Zhi, Y. Bando, C. Tang, H. Kuwahara, D. Golberg, *Adv. Mater.* **2009**, *21*, 2889.
[204] E. Husain, T. N. Narayanan, J. J. Taha-Tijerina, S. Vinod, R. Vajtai, P. M. Ajayan, *Acs Appl. Mater. Interfaces* **2013**, *5*, 4129.
[205] M. Yi, Z. Shen, W. Zhang, J. Zhu, L. Liu, S. Liang, X. Zhang, S. Ma, *Nanoscale* **2013**, *5*, 10660.
[206] L. Liu, Z. Shen, Y. Zheng, M. Yi, X. Zhang, S. Ma, *RSC Advances* **2014**, *4*, 37726.
[207] M. Yi, Z. Shen, X. Zhao, S. Liang, L. Liu, *Appl. Phys. Lett.* **2014**, *104*, 143101.
[208] M. Yi, Z. Shen, L. Liu, S. Liang, *RSC Adv* **2015**, *5*, 2983.
[209] J. Yu, Y. Chen, R. G. Elliman, M. Petravic, *Adv. Mater.* **2006**, *18*, 2157.
[210] C. Harrison, S. Weaver, C. Bertelsen, E. Burgett, N. Hertel, E. Grulke, *J. Appl. Polym. Sci.* **2008**, *109*, 2529.
[211] K. Watanabe, T. Taniguchi, T. Niiyama, K. Miya, M. Taniguchi, *Nat. Photonics* **2009**, *3*, 591.
[212] P. Bharadwaj, M. Parzefall, A. Jain, T. Taniguchi, K. Watanabe, L. Novotny, *Nat. Nanotechnol.* **2015**, *10*, 1058.
[213] K. Watanabe, T. Taniguchi, H. Kanda, *Nat. Mater.* **2004**, *3*, 404.
[214] K. Watanabe, T. Taniguchi, H. Kanda, *Phys. Status Solidi A* **2004**, *201*, 2561.
[215] J. Li, S. Majety, R. Dahal, W. P. Zhao, J. Y. Lin, H. X. Jiang, *Appl. Phys. Lett.* **2012**, *101*, 171112.
[216] H. Wang, X. Zhang, H. Liu, Z. Yin, J. Meng, J. Xia, X. M. Meng, J. Wu, J. You, *Adv. Mater.* **2015**, *27*, 8109.
[217] J. D. Caldwell, A. V. Kretinin, Y. Chen, V. Giannini, M. M. Fogler, Y. Francescato, C. T. Ellis, J. G. Tischler, C. R. Woods, A. J. Giles, M. Hong, K. Watanabe, T. Taniguchi, S. A. Maier, K. S. Novoselov, *Nat. Commun.* **2014**, *5*, 5221.
[218] P. Li, M. Lewin, A. V. Kretinin, J. D. Caldwell, K. S. Novoselov, T. Taniguchi, K. Watanabe, F. Gaussmann, T. Taubner, *Nat. Commun.* **2015**, *6*, 7507.
[219] L. Ju, J. VelascoJr, E. Huang, S. Kahn, C. Nosiglia, H.-Z. Tsai, W. Yang, T. Taniguchi, K. Watanabe, Y Zhang, G. Zhang, M. Crommie, A. Zettl, F. Wang, *Nat. Nanotechnol.* **2014**, *9*, 348.
[220] T. T. Tran, K. Bray, M. J. Ford, M. Toth, I. Aharonovich, *Nat. Nanotechnol.* **2015**, *11*, 37.
[221] S. Liu, B. Lu, Q. Zhao, J. Li, T. Gao, Y. Chen, Y. Zhang, Z. Liu, Z. Fan, F. Yang, L. You, D. Yu, *Adv. Mater.* **2013**, *25*, 4549.
[222] H. Zeng, C. Zhi, Z. Zhang, X. Wei, X. Wang, W. Guo, Y. Bando, D. Golberg, *Nano Lett.* **2010**, *10*, 5049.
[223] K. J. Erickson, A. L. Gibb, A. Sinitskii, M. Rousseas, N. Alem, J. M. Tour, A. K. Zettl, *Nano Lett.* **2011**, *11*, 3221.
[224] A. Sinitskii, K. J. Erickson, W. Lu, A. L. Gibb, C. Zhi, Y. Bando, D. Golberg, A. Zettl, J. M. Tour, *ACS Nano* **2014**, *8*, 9867.
[225] L. Li, L. H. Li, Y. Chen, X. J. Dai, P. R. Lamb, B.-M. Cheng, M.-Y. Lin, X. Liu, *Angew. Chemie* **2013**, *125*, 4306.
[226] A. Fathalizadeh, T. Pham, W. Mickelson, A. Zettl, *Nano Lett.* **2014**, *14*, 4881.
[227] R. Mukherjee, S. Bhowmick, *J. Chem. Theory Comput.* **2011**, *7*, 720.
[228] L. Lai, J. Lu, L. Wang, G. Luo, J. Zhou, R. Qin, Z. Gao, W. N. Mei, *J. Phys. Chem. C* **2009**, *113*, 2273.
[229] Z. Zhang, W. Guo, *Phys. Rev. B* **2008**, *77*, 075403.
[230] S. Wang, Q. Chen, J. Wang, *Appl. Phys. Lett.* **2011**, *99*, 063114.
[231] Z. Zhang, W. Guo, B. I. Yakobson, *Nanoscale* **2013**, *5*, 6381.
[232] V. Barone, J. E. Peralta, *Nano Lett.* **2008**, *8*, 2210.
[233] E. Kan, F. Wu, H. Xiang, J. Yang, M.-H. Whangbo, *J. Phys. Chem. C* **2011**, *115*, 17252.
[234] A. Lopez-Bezanilla, J. Huang, H. Terrones, B. G. Sumpter, *Nano Lett.* **2011**, *11*, 3267.
[235] F. Zheng, G. Zhou, Z. Liu, J. Wu, W. Duan, B.-L. Gu, S. B. Zhang, *Phys. Rev. B* **2008**, *78*, 205415.
[236] W. Chen, Y. Li, G. Yu, C.-Z. Li, S. B. Zhang, Z. Zhou, Z. Chen, *J. Am. Chem. Soc.* **2010**, *132*, 1699.
[237] J. Qi, X. Qian, L. Qi, J. Feng, D. Shi, J. Li, *Nano Lett.* **2012**, *12*, 1224.
[238] C. Feng, Z. Mi, Z. Jian-Xin, *Chin. Phys. B* **2010**, *19*, 086105.
[239] Z.-X. Xie, L.-M. Tang, C.-N. Pan, Q. Chen, K.-Q. Chen, *J. Appl. Phys.* **2013**, *114*, 144311.
[240] E. Hernández, C. Goze, P. Bernier, A. Rubio, *Phys. Rev. Lett.* **1998**, *80*, 4502.
[241] H. F. Bettinger, T. Dumitric , G. E. Scuseria, B. I. Yakobson, *Phys. Rev. B* **2002**, *65*, 041406.
[242] T. Dumitrič, B. I. Yakobson, *Phys. Rev. B* **2005**, *72*, 035418.
[243] Y. Dai, W. Guo, Z. Zhang, B. Zhou, C. Tang, *J. Phys. D: Appl. Phys.* **2009**, *42*, 085403.
[244] X. Blase, A. Rubio, S. Louie, M. Cohen, *Euro. Phys. Lett.* **1994**, *28*, 335.
[245] C. Zhi, Y. Bando, C. Tang, D. Golberg, R. Xie, T. Sekigushi, *Appl. Phys. Lett.* **2005**, *86*, 213110.
[246] J. Wu, W.-Q. Han, W. Walukiewicz, J. W. Ager, W. Shan, E. E. Haller, A. Zettl, *Nano Lett.* **2004**, *4*, 647.
[247] M. Terauchi, M. Tanaka, K. Suzuki, A. Ogino, K. Kimura, *Chem. Phys. Lett.* **2000**, *324*, 359.
[248] Z. Zhang, W. Guo, Y. Dai, *J. Appl. Phys.* **2009**, *105*, 084312.
[249] J. Yu, D. Yu, Y. Chen, H. Chen, M.-Y. Lin, B.-M. Cheng, J. Li, W. Duan, *Chem. Phys. Lett.* **2009**, *476*, 240.
[250] Z. Zhang, W. Guo, Y. Dai, *Appl. Phys. Lett.* **2008**, *93*, 223108.
[251] L. Wirtz, A. Marini, A. Rubio, *Phys. Rev. Lett.* **2006**, *96*, 126104.
[252] K. H. Khoo, M. S. C. Mazzoni, S. G. Louie, *Phys. Rev. B* **2004**, *69*, 201401.
[253] C.-W. Chen, M.-H. Lee, S. Clark, *Nanotechnology* **2004**, *15*, 1837.
[254] C. Tang, Y. Bando, Y. Huang, S. Yue, C. Gu, F. Xu, D. Golberg, *J. Am. Chem. Soc.* **2005**, *127*, 6552.
[255] Z. Zhang, W. Guo, *J. Am. Chem. Soc.* **2009**, *131*, 6874.
[256] Z. Zhang, X. C. Zeng, W. Guo, *Phys. Rev. B* **2010**, *82*, 035412.
[257] D. Golberg, Y. Bando, K. Kurashima, T. Sato, *Solid State Commun.* **2000**, *116*, 1.
[258] S. Okada, S. Saito, A. Oshiyama, *Phys. Rev. B* **2002**, *65*, 165410.
[259] Z.-H. Zhang, W.-L. Guo, B. I. Yakobson, *Acta Mech. Sinica* **2012**, *28*, 1532.
[260] R. H. Wentorf, *J. Chem. Phys.* **1957**, *26*, 956.
[261] T. Ishii, T. Sato, Y. Sekikawa, M. Iwata, *J. Cryst. Growth* **1981**, *52*, 285.
[262] M. Topsakal, E. Aktürk, S. Ciraci, *Phys. Rev. B* **2009**, *79*, 115442.
[263] M. Wu, X. Wu, Y. Pei, Y. Wang, X. C. Zeng, *Chem. Commun.* **2011**, *47*, 4406.
[264] S. Zhang, Q. Wang, Y. Kawazoe, P. Jena, *J. Am. Chem. Soc.* **2013**, *135*, 18216.
[265] B. Albert, H. Hillebrecht, *Angew. Chem. Int. Ed.* **2009**, *48*, 8640.
[266] A. P. Sergeeva, I. A. Popov, Z. A. Piazza, W. L. Li, C. Romanescu, L. S. Wang, A. I. Boldyrev, *Acc. Chem. Res.* **2014**, *47*, 1349.
[267] B. E. Douglas, S. M. Ho, *Structure and Chemistry of Crystalline Solids*, Springer, N.Y., **2006**.
[268] T. Ogitsu, E. Schwegler, G. Galli, *Chem. Rev.* **2013**, *113*, 3425.
[269] A. R. Oganov, J. H. Chen, C. Gatti, Y. Z. Ma, Y. M. Ma, C. W. Glass, Z. X. Liu, T. Yu, O. O. Kurakevych, V. L. Solozhenko, *Nature* **2009**, *457*, 863.
[270] M. H. Evans, J. D. Joannopoulos, S. T. Pantelides, *Phys. Rev. B* **2005**, *72*, 045434.
[271] J. Kunstmann, A. Quandt, *Phys. Rev. B* **2006**, *74*, 035413.

[272] W. L. Li, Q. Chen, W. J. Tian, H. Bai, Y. F. Zhao, H. S. Hu, J. Li, H. J. Zhai, S. D. Li, L. S. Wang, *J. Am. Chem. Soc.* **2014**, *136*, 12257.
[273] Z. A. Piazza, H. S. Hu, W. L. Li, Y. F. Zhao, J. Li, L. S. Wang, *Nat. Commun.* **2014**, *5*, 3113.
[274] X. F. Zhou, X. Dong, A. R. Oganov, Q. Zhu, Y. J. Tian, H. T. Wang, *Phys. Rev. Lett.* **2014**, *112*, 085502.
[275] X. F. Zhou, A. R. Oganov, X. Shao, Q. Zhu, H. T. Wang, *Phys. Rev. Lett.* **2014**, *113*, 176101.
[276] X. J. Wu, J. Dai, Y. Zhao, Z. W. Zhuo, J. L. Yang, X. C. Zeng, *ACS Nano* **2012**, *6*, 7443.
[277] J. L. He, E. D. Wu, H. T. Wang, R. P. Liu, Y. J. Tian, *Phys. Rev. Lett.* **2005**, *94*, 015504.
[278] H.-J. Zhai, Y.-F. Zhao, W.-L. Li, Q. Chen, H. Bai, H.-S. Hu, Z. A. Piazza, W.-J. Tian, H.-G. Lu, Y.-B. Wu, Y.-W. Mu, G.-F. Wei, Z.-P. Liu, J. Li, S.-D. Li, L.-S. Wang, *Nat. Chem.* **2014**, *6*, 727.
[279] C. J. Otten, O. R. Lourie, M. F. Yu, J. M. Cowley, M. J. Dyer, R. S. Ruoff, W. E. Buhro, *J. Am. Chem. Soc.* **2002**, *124*, 4564.
[280] F. Liu, J. F. Tian, L. H. Bao, T. Z. Yang, C. M. Shen, X. Y. Lai, Z. M. Xiao, W. G. Xie, S. Z. Deng, J. Chen, J. C. She, N. S. Xu, H. J. Gao, *Adv. Mater.* **2008**, *20*, 2609.
[281] C. H. Lin, H. Ni, X. N. Wang, M. Chang, Y. J. Chao, J. R. Deka, X. D. Li, *Small* **2010**, *6*, 927.
[282] L. M. Cao, Z. Zhang, L. L. Sun, C. X. Gao, M. He, Y. Q. Wang, Y. C. Li, X. Y. Zhang, G. Li, J. Zhang, W. K. Wang, *Adv. Mater.* **2001**, *13*, 1701.
[283] J. Miller, *Phys. Today* **2007**, *60*, 20.
[284] J. Kunstmann, V. Bezugly, H. Rabbel, M. H. Rummeli, G. Cuniberti, *Adv. Funct. Mater.* **2014**, *24*, 4127.
[285] T. T. Xu, J.-G. Zheng, Wu, A. W. Nicholls, J. R. Roth, D. A. Dikin, R. S. Ruoff, *Nano Lett.* **2004**, *4*, 963.
[286] J. Xu, Y. Chang, L. Gan, Y. Ma, T. Zhai, *Adv. Sci.* **2015**, *2*, 1500023.
[287] E. S. Penev, S. Bhowmick, A. Sadrzadeh, B. I. Yakobson, *Nano Lett.* **2012**, *12*, 2441.
[288] Y. Y. Liu, E. S. Penev, B. I. Yakobson, *Angew. Chem. Int. Ed.* **2013**, *52*, 3156.
[289] Z. H. Zhang, Y. Yang, G. Y. Gao, B. I. Yakobson, *Angew. Chem. Int. Ed.* **2015**, *54*, 13022.
[290] X.-F. Zhou, O. R. Oganoa, Z. Wang, I. A. Popov, A. I. Boldyrev, H.-T. Wang,*Phys. Rev. B* **2016**, *93*, 085406.
[291] A. J. Mannix, X.-F. Zhou, B. Kiraly, J. D. Wood, D. Alducin, B. D. Myers, X. Liu, B. L. Fisher, U. Santiago, J. R. Guest, M. J. Yacaman, A. Ponce, A. R. Oganov, M. C. Hersam, N. P. Guisinger, *Science* **2015**, *350*, 1513.
[292] B. Feng, J. Zhang, Q. Zhong, W. Li, S. Li, H. Li, P. Cheng, S. Meng, L. Chen, K. Wu, *arXiv preprint arXiv:1512.05029,* **2015**.
[293] B. Feng, J. Zhang, R.-Y. Liu, I. Takushi, C. Lian, L. Chen, K. Wu, H. Li, S. Meng, F. Komori, *arXiv preprint arXiv:1512.05270*, **2015**.
[294] S. H. Zhang, Y. W. Li, T. S. Zhao, Q. Wang, *Sci. Rep.* **2014**, *4*, 5241.
[295] B. Meng, W. Z. Xiao, L. L. Wang, L. Yue, S. Zhang, H. Y. Zhang, *RSC Adv.* **2015**, *5*, 82357.

Received: January 6, 2016
Revised: February 26, 2016
Published online: April 13, 2016